*Human Molecular Genetics, 2013, Vol. 22, No. 10* **2024–2040**
*doi:10.1093/hmg/ddt054*
*Advance Access published on February 7, 2013*

# The Meckel syndrome protein meckelin (*TMEM67*) is a key regulator of cilia function but is not required for tissue planar polarity

**Amanda C. Leightner[1], Cynthia J. Hommerding[2], Ying Peng[1], Jeffrey L. Salisbury[1], Vladimir G. Gainullin[1], Peter G. Czarnecki[2,†], Caroline R. Sussman[3] and Peter C. Harris[1,2,*]**

[1]Department of Biochemistry and Molecular Biology, [2]Division of Nephrology and Hypertension, Department of Medicine and [3]Department of Physiology and Biomedical Engineering, Mayo Clinic, Rochester, MN, USA

Received October 8, 2012; Revised January 10, 2013; Accepted February 4, 2013

**Meckel syndrome (MKS) is a lethal disorder associated with renal cystic disease, encephalocele, ductal plate malformation and polydactyly. MKS is genetically heterogeneous and part of a growing list of syndromes called ciliopathies, disorders resulting from defective cilia. *TMEM67* mutation (MKS3) is a major cause of MKS and the related ciliopathy Joubert syndrome, although the complete etiology of the disease is not well understood. To further investigate MKS3, we analyzed phenotypes in the *Tmem67* null mouse (*bpck*) and in zebrafish *tmem67* morphants. Phenotypes similar to those in human MKS and other ciliopathy models were observed, with additional eye, skeletal and inner ear abnormalities characterized in the *bpck* mouse. The observed disorganized stereociliary bundles in the *bpck* inner ear and the convergent extension defects in zebrafish morphants are similar to those found in planar cell polarity (PCP) mutants, a pathway suggested to be defective in ciliopathies. However, analysis of classical vertebrate PCP readouts in the *bpck* mouse and ciliary organization analysis in *tmem67* morphants did not support a global loss of planar polarity. Canonical Wnt signaling was upregulated in cyst linings and isolated fibroblasts from the *bpck* mouse, but was unchanged in the retina and cochlea tissue, suggesting that increased Wnt signaling may only be linked to MKS3 phenotypes associated with elevated proliferation. Together, these data suggest that defective cilia loading, but not a global loss of ciliogenesis, basal body docking or PCP signaling leads to dysfunctional cilia in MKS3 tissues.**

## INTRODUCTION

Cilia are highly conserved microtubule-based organelles that protrude from the apical surface of most cells. The core structure of cilia, the axoneme, is nucleated and extended out of a modified centriole called the basal body. The axoneme is a ring of nine microtubule doublets that is ensheathed by a membrane contiguous with the plasma membrane (1–4). Cilia can be either motile or non-motile. Specialized motile cilia are found at the embryonic node and generate a leftward fluid flow responsible for left–right body symmetry. Motile cilia are also present in respiratory epithelia, brain ependymal cells and epithelial cells lining the fallopian tubes, where they are responsible for generating flow (3). Primary cilia are specialized immotile cilia, present at a ratio of one per cell, and are thought to have mechanosensory functions. In addition, primary cilia may play a role in mediating signaling events involved in development, such as Sonic Hedgehog (Shh), Wnt signaling (canonical and non-canonical) and cell-cycle signaling events (1,2,5).

Primary cilium disruption can lead to the development of a set of disorders called ciliopathies. The ciliopathies encompass several syndromes including nephronophthisis (NPHP), Joubert syndrome (JBTS), Bardet Biedl syndrome (BBS) and Meckel syndrome (MKS) (6). Proteins associated with ciliopathies are primarily localized to the basal body or primary cilium, suggesting the proteins share common functions to preserve cilia and basal body structure, function and protein composition

*To whom correspondence should be addressed at: Division of Nephrology and Hypertension, Mayo Clinic, 200 First Street SW, Rochester, MN 55905, USA. Tel: +1 5072660541; Fax: +1 5072669315; Email: harris.peter@mayo.edu
†Present address: Division of Nephrology, Beth Israel Deaconess Medical Center, Boston, MA, USA.

(2,7–10). The ciliopathies have a high degree of genetic and phenotypic overlap, especially NPHP, JBTS and MKS, suggesting that these syndromes represent variants of a related disease with differing phenotypic severity, dependent on allelic effects, genetic complexity and genetic background (1,4,6,11–13).

MKS is the most severe ciliopathy, being embryonic lethal by definition. It is relatively rare in outbred populations with the most common phenotypes being renal cystic dysplasia, central nervous system defects, usually occipital encephalocele, hepatic ductal plate malformations and polydactyly (4,14,15). At least 10 loci have been associated with typical MKS, including *MKS1* (16), *TMEM216* (17), *TMEM67* (MKS3, Meckel syndrome type 3, OMIM 607361) (18), *CEP290* (19), *RPGRIP1L* (20), *CC2D2A* (21), *TCTN2* (22), *B9D1* (23), *B9D2* (24) and *NPHP3* (25). Our studies focus on the *TMEM67* locus, which is one of the most common causes of MKS and is also associated with JBTS and NPHP (26–29). The resulting product, meckelin, is a proposed 7-transmembrane receptor-like protein with few defined domains, but contains an extracellular cysteine-rich region (18). A number of protein complexes containing MKS, JBTS and NPHP proteins have recently been described (7,8,12,30–32). These complexes have been localized to a specialized region of the cilium called the transition zone and are proposed to regulate ciliary membrane protein composition (7,11). Meckelin has been localized to one of these complexes, the 'MKS-B9' complex. In addition, meckelin depletion was shown to regulate centrosome number and cilia length in animal and cell models (33,34).

Several signaling pathways, including the developmental Wnt signaling cascades, are suggested to require a functional cilium for normal levels of signaling; however, the pathway relationship with PKD and the ciliopathies remains controversial (35). Wnt signaling has two major arms, the canonical (Wnt) and non-canonical pathways, including the planar cell polarity (PCP) pathway. Canonical Wnt signaling is dependent on the transcription factor β-catenin, which functions as a transcription co-factor to regulate cell proliferation and differentiation events (36). Canonical Wnt signaling has been described as upregulated in PKD and transgenic mice overexpressing an activated form of β-catenin develop cystic disease, linking elevated canonical Wnt signaling to increased proliferation rates and cystogenesis (37–40). The primary cilium may modulate canonical Wnt signaling levels through sequestration of signaling components such as β-catenin at the basal body, causing decreased nuclear translocation and transcriptional activity (39).

The PCP pathway, in contrast, is suggested to be downregulated in PKD and the ciliopathies. PCP controls cellular polarization within a plane perpendicular to the apical-basal axis and employs cellular interactions to coordinate polarization among neighboring cells (41,42). A set of core PCP proteins were identified from *Drosophilia* studies including: *frizzled* (*fz*), *dishevelled* (*dsh*), *prickle* (*pk*), *van gogh/strabismus* (*vang/stbm*), *flamingo* (*fmi*) and *diego* (*dgo*) (43). These proteins become asymmetrically distributed to the distal and proximal cell membranes for planar polarization to occur (42,44). A set of homologous PCP proteins in vertebrates are involved in convergent extension (CE), which controls polarized cell movements leading to narrowing and lengthening of tissues, including elongation of the anterior–posterior axis during gastrulation and neural tube development (45,46). Besides CE, several vertebrate phenotypes have been used to assess disruption of PCP signaling, including uniform orientation of actin-based stereociliary bundles and the kinocilium, a specialized primary cilium in the organ of Corti (OC) of the inner ear (46). In addition, PCP has also been shown to play important roles in orienting the axis of mitotic spindles during cell division in developing tissues (47). Defective mitotic spindle orientation in developing renal tubules of rodent PKD models has been linked to defective PCP and cystogenesis; however, the importance for cyst initiation remains controversial (42,48–50).

In this study, we utilized zebrafish *tmem67* ciliopathy morphants and the null *Tmem67* (*bpck*) mouse model (51) to explore the role of meckelin in cilia maintenance and functionality in various organs, including examination of potential defects in canonical Wnt and PCP output.

## RESULTS

### Renal phenotypes in the *bpck* mouse model

To better understand the tissue-specific requirement for meckelin in cilia maintenance and functioning, we first examined the extent and progression of kidney cystogenesis in the *bpck* mouse, a spontaneous mutant with all of *Tmem67* removed (51). The *bpck* phenotypes are similar to human MKS3 and the *wpk* rat model of this disease (18,26,27,52). However, many MKS3 phenotypes, especially the extrarenal phenotypes, have not been characterized in detail. For these studies, we inbred the original *bpck* mouse from a B6C3FeF1/J*a/a* mixed background into C57BL6/J and compared the severity of cystic disease to the original outbred background. In the outbred state, mild cystic tubule dilation was observed as early as embryonic day (E)16.5 in *bpck* mice (Fig. 1A). Cysts became more pronounced by postnatal day (P)1, with cystogenesis in the inbred animal more severe than the outbred state (Fig. 1B and D). Comparison of disease severity near the end of lifespan of outbred (P16) and inbred mice (P13; Fig. 1C and E) showed widespread cystogenesis that was more extensive in the younger inbred animal. Staining for cystic tubule origin at P12 showed that the largest cysts were derived from the collecting duct, with occasional dilation of the proximal tubule and loop of Henle (Fig. 1F and G; average cyst diameter: collecting ducts = 1018 μm, 1889 tubules; proximal tubules = 470 μm, 1113 tubules; loop of Henle = 84 μm, 1078 tubules). Additionally, *bpck* mice displayed a survival disadvantage in both outbred and inbred states. While the level of outbred *bpck* mice was normal at P1, it dropped well below the expected 25% by P4, while in the inbred state survival dropped below the expected level beginning at E18.5 with only rare liveborn mutants (Fig. 1H and I, Supplementary Material, Table S1).

### Extrarenal phenotypes in *bpck* mice

Meckelin requirement for cilia maintenance was next examined in extrarenal tissues. Retinal sections from P16 outbred *bpck* animals displayed severe retinal degeneration, as seen by thinning of both the inner and outer retinal segments (Supplementary Material, Fig. S1A). Higher resolution analysis of the tissue by transmission electron microscopy (TEM)

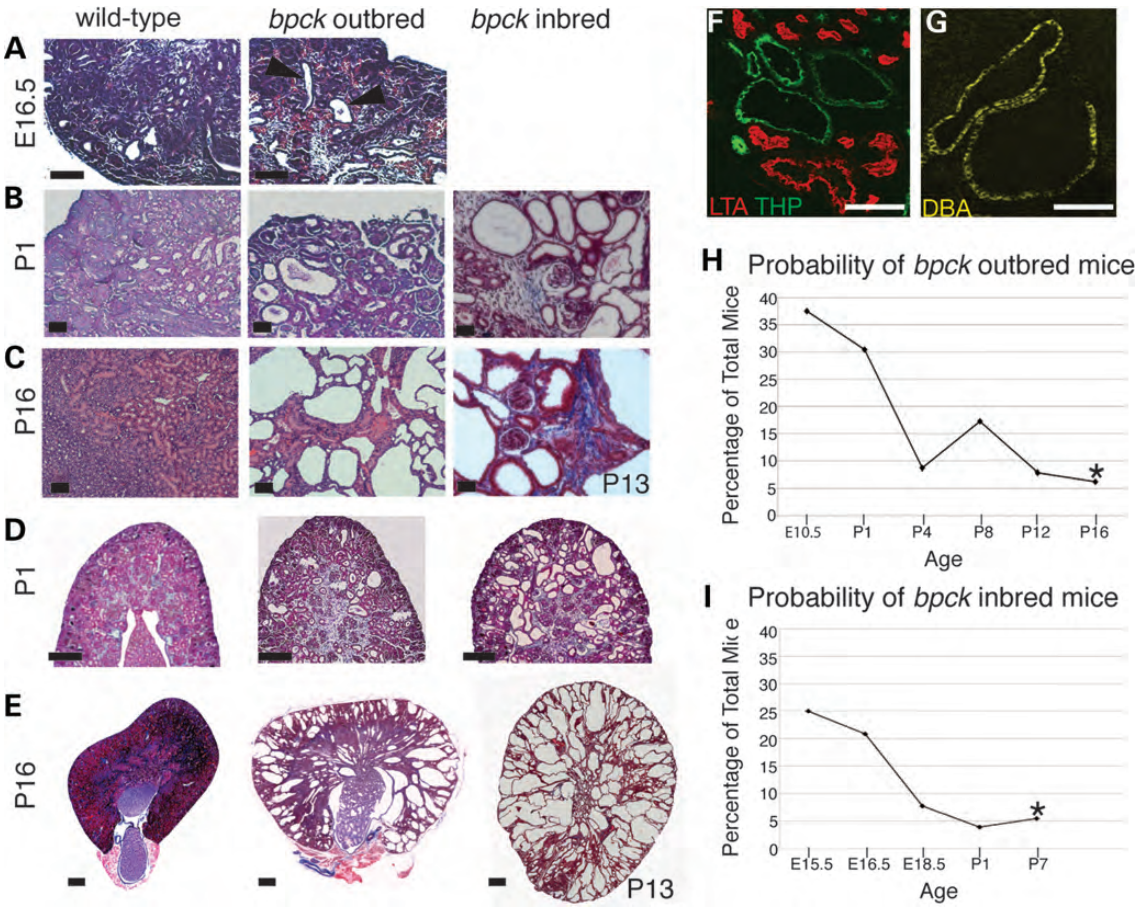


**Figure 1.** Depletion of meckelin in the *bpck* mouse leads to polycystic kidney disease (PKD). Mallory SS trichrome stained kidney sections at high (**A**–**C**) and low magnification (**D**, **E**) of (A) E16.5, (B, D) P1 and (C, E) P16 (outbred), P13 (inbred) comparing wild-type and inbred and outbred *bpck*. Arrowheads in (A) indicate dilated tubules. Scale bar in (A–C) is 20 μm and 100 μm in (D) and (E). (**F**) LTA (lotus tetragonolobus agglutinin; proximal tubules) and THP (Tamm-Horsfall protein; loop of Henle) staining, plus (**G**) DBA (Dolichos biflorus; collecting ducts) labeling in P12 outbred *bpck* kidney sections (scale bar = 100 μm). Survival analysis of (**H**) outbred and (**I**) inbred *bpck* mutants (Supplementary Material, Table S1). Insufficient numbers of inbred P13 *bpck* mice survived for accurate analysis. Statistics are based on a two-tailed Fisher's exact test. $^{*}P < 0.05$.

revealed a general disorganization of retinal layers in *bpck* mice with no structurally identifiable outer segment, as seen with the disc-shaped rod cells in the wild-type retina (Fig. 2A). However, the connecting cilium was present in *bpck* retinas and appeared structurally similar to the wild-type (Fig. 2A, inserts). Functionality of the connecting cilium was examined via transport of the G-coupled protein receptor rhodopsin in retinal segments. In wild-type tissue, rhodopsin was transported to the outer segment; however, in the *bpck* retina, rhodopsin accumulated in the inner segment and outer nuclear layer (Fig. 2B). Apoptotic rates were increased in the outer nuclear layer and inner and outer segments of the retina in P12 and P16 *bpck* mice (Supplementary Material, Fig. S1B and C), suggesting that the loss of protein transport along the connecting cilium leads to death of retinal cell layers, and underlies the degenerative phenotype.

Skeletal abnormalities such as postaxial polydactyly, club-feet and short limbs have been documented in MKS, although may be rare in MKS3 patients (14,26,27). In addition, mouse models of *Mks1* display a range of skeletal deformations, prompting us to analyze meckelin functioning during skeletal development (53,54). Gross examination of E16.5 skeletons showed no overt malformations in *bpck* mice, including normal ossification of vertebrate bodies and no clear evidence of cleft palate (Supplementary Material, Fig. S1D–F). Forelimb development was also normal, with no evidence of polydactyly (5/5 *bpck* mice; Supplementary Material, Fig. S2G and H). However, fibula bones had a significant bowing in all mutants examined (5/5), and the fibula, tibia and femur were slightly shorter than the wild-type, although not reaching statistical significance (Fig. 2C and D). This verifies that although Mks1 and meckelin may be involved in similar complexes, they play divergent roles in different primary cilia-dependent developmental processes (26,27,33).

Lastly, the function of meckelin in cilia maintenance in multiciliated respiratory cells in P1 mouse trachea was examined. Meckelin removal did not affect docking of the basal body onto the apical cell surface in *bpck* mice, and the cilia appeared structurally normal compared with the wild-type (Fig. 2E). The average density of respiratory cilia was not significantly different between mutants and wild-type littermates, although cilia density was more variable in mutant mice (Fig. 2F; wild-type sd = 0.215, *bpck* sd = 1.65). Our results demonstrate that basal body trafficking and docking are

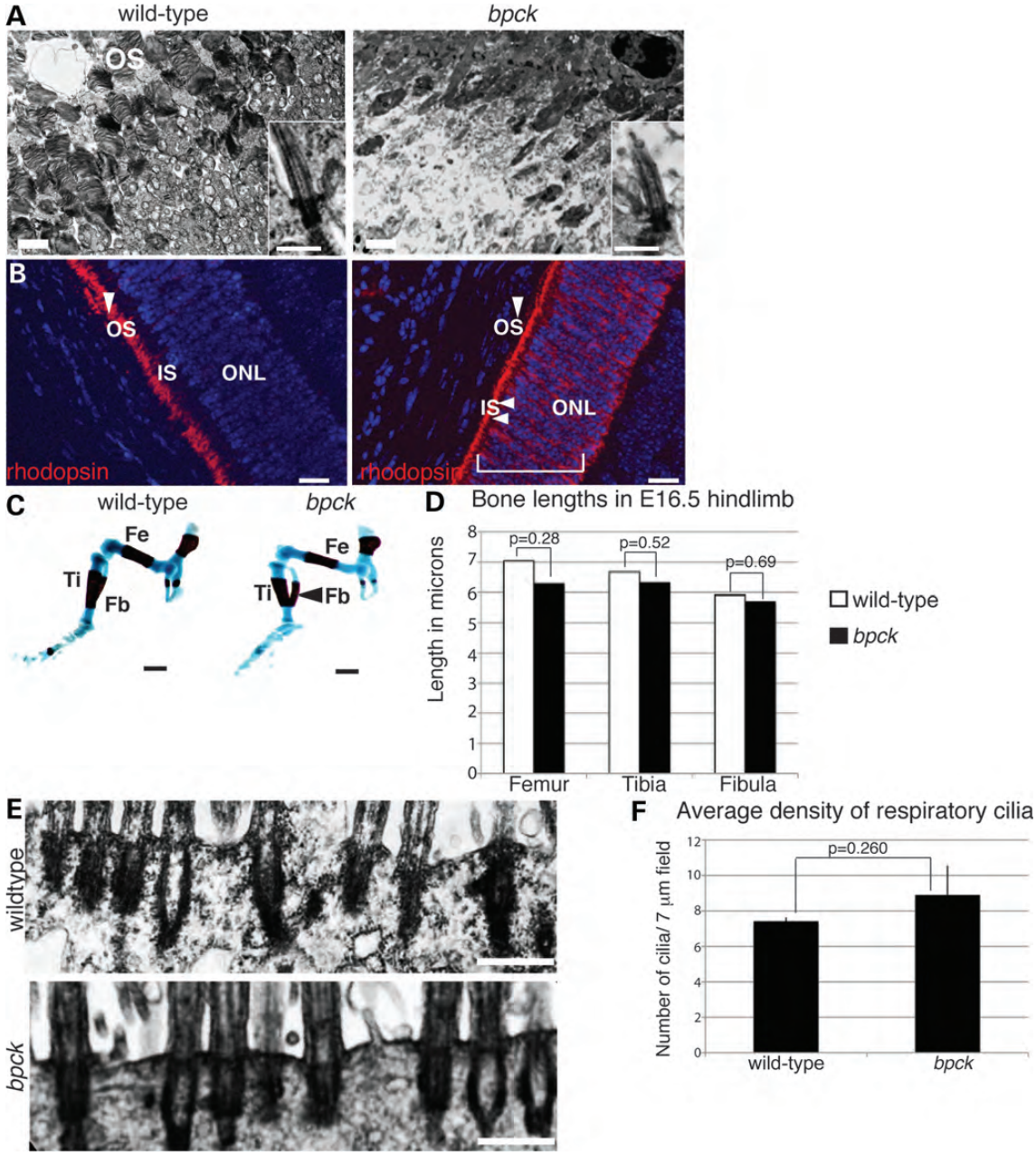


**Figure 2.** *bpck* mice display extrarenal abnormalities. (**A**) TEM images of P12 outbred retinal sections (scale bar = 2 μm). Inserts show the connecting cilium (scale bar = 0.5 μm). OS, outer segment. (**B**) Rhodopsin transport to the outer segment (arrowhead) in P12 mice. ONL, outer nuclear layer; IS, inner segment (double arrowheads). Scale bar = 20 μm. (**C**) Skeletal staining of E16.5 mice with lateral view of the hindlimbs with bowed fibula in mutant (arrowhead). Fe, femur; Ti, tibia; Fb, fibula. Scale bar = 2 mm. Alizarin red staining indicates mineralized bone and alcian blue shows cartilage. (**D**) Quantitation of bone lengths in the hindlimb ($n = 3$ wild-type, 2 *bpck*). (**E**) TEM images of P1 respiratory cilia in mouse trachea. Scale bar = 0.5 μm. (**F**) Quantitation of respiratory cilia density in P1 mouse trachea ($n = 2$ wild-type, 3 *bpck*). Statistics in (D, F) based on Student's *t*-test.

largely unaffected by meckelin loss, at least in multiciliated airway epithelial cells. This is in contrast to previous *in vitro* studies where transient meckelin depletion led to apparent apical basal body docking defects (34,55).

### *Tmem67* deletion results in ciliogenesis and hair cell orientation defects in the OC

We next investigated the effects of meckelin depletion on formation and maintenance of another specialized primary cilium, the kinocilium, in the inner ear of *bpck* mice. Oriented alignment of the 'V'-shaped stereociliary bundles in sensory hair cells in the cochlea of the inner ear is a robust demonstration of planar polarization of the underlying sensory epithelium. Thus, deregulation of hair cell alignment in other ciliopathy models has been interpreted as a PCP-dependent defect (56). Hair cell orientation was examined in cochleae from P1 littermates by scanning electron microscopy (SEM). Cell alignment was analyzed by measuring the degree of rotation of the stereociliary bundle from the lateral tissue edge in

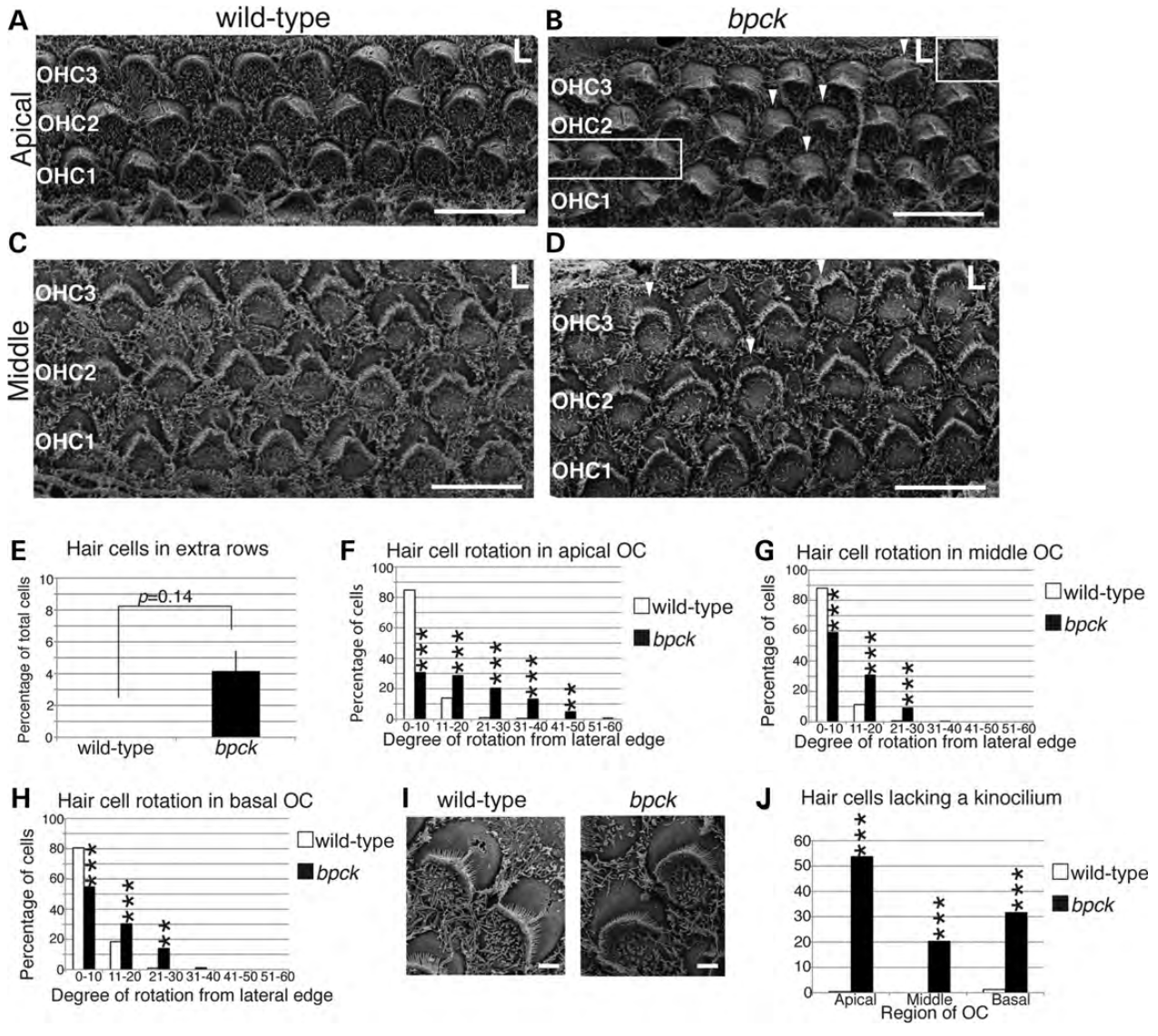


**Figure 3.** Meckelin disruption leads to ciliogenesis and 'PCP-like' phenotypes in the OC of the inner ear. Hair cells in the three outer hair cell (OHC) rows were analyzed by SEM in all regions of the OC in P1 mice. Rows of OHCs in (**A**) wild-type and (**B**) *bpck* apical regions of the OC. L, lateral edge of the tissue. Arrows indicate abnormally shaped stereociliary bundles and cells with rotational defects from the lateral edge, and the boxed areas illustrate additional rows of stereociliary bundles. Hair cells in the middle region of the (**C**) wild-type and (**D**) *bpck* OC (scale bar in A–D = 10 μm). (**E**) Quantitation of percentage of hair cells in P1 OC in extra rows. ($n = 2$ wild-type, 2 *bpck* mice, ~200 cells/genotype). Statistics based on two-tailed Student's *t*-test. Quantitation of stereociliary bundle rotation from the lateral edge in (**F**) apical, (**G**) middle and (**H**) basal regions of the OC ($n = 2$ wild-type, 2 *bpck* mice). Approximately 90–200 cells were analyzed in each region of the OC. (**I**) High-resolution images of hair cells with or without kinocilia in wild-type or *bpck* OC (scale bar = 1 μm). (**J**) Quantitation of kinocilia absence in OC rows ($n = 2$ wild-type, 2 *bpck* mice). Between 100 and 200 cells were analyzed in each region of the OC. $^{***}P \leq 0.0001$, $^{**}P < 0.01$ based on a two-tailed Fisher's exact test (in F–H, J).

the apical, middle and basal regions of the OC, the sensory portion of the cochlea. We found the gross alignment of stereocilia across the tissue to be largely intact, although frequent morphological and orientation defects were observed within individual hair cells (Fig. 3A–D and F–H). Hair cells in apical regions of the OC were the most disorganized in *bpck* mice, with many stereociliary bundles displaying abnormal or flattened morphology (Fig. 3A and B), with statistically significant stereociliary alignment defects (Fig. 3F). Extra rows of hair cells were present in this region and throughout the OC, as observed in PCP mouse mutants, likely due to cochlear CE defects (Fig. 3B) (57,58). However, the percentage of hair cells present in extra rows in the *bpck* OC did not reach statistical significance compared with wild-type controls (Fig. 3E), showing that the *bpck* OC is not as disorganized as in PCP mutants with CE defects. Cells were also disorganized in the middle and basal OC, with some stereociliary bundles having an abnormal 'U'-shaped morphology (Fig. 3C and D). Rotational defects also occurred in middle and basal OC regions, but were not as severe as in the apex (Fig. 3G and H).

Furthermore, we found a significant proportion of *bpck* hair cells lacked a kinocilium in all regions of the OC, while these defects were rarely observed in wild-type mice. The highest

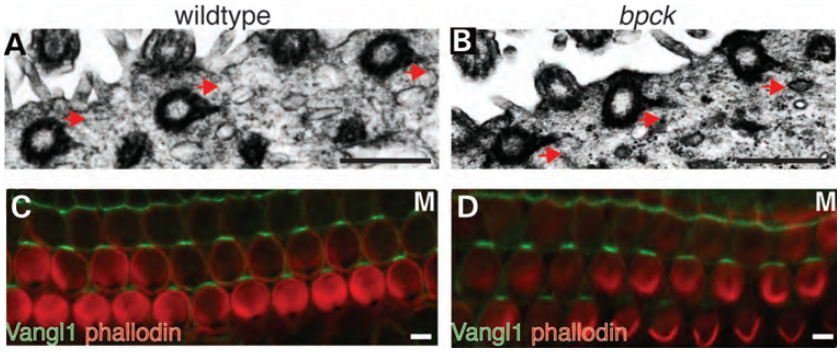


**Figure 4.** Classical PCP signaling is maintained in *bpck* mice. TEM imaging of P1 (**A**) wild-type and (**B**) *bpck* tracheal tissue showing orientation of basal feet (arrows). Scale bar = 0.5 μm. Localization of the core PCP protein Vangl1 in P1 (**C**) wild-type and (**D**) *bpck* OHCs (M, medial edge). Scale bar = 5 μm. Stereociliary bundles are stained with phallodin.

percentage of ciliogenesis defects occurred in the apical region with somewhat milder defects in the middle and basal regions of the OC (Fig. 3I and J). The mild orientation defects in the *bpck* mice resemble those seen in the ciliopathy BBS or ciliary *Kif3a* models (56,59), but differ markedly in degree from the much greater misorientation found in core PCP mouse mutants, such as in $Vangl2^{Lp/Lp}$ animals where the stereocilia orientation can reach 120° (57,58,60). These data, along with data from other ciliopathy models, suggest that input may be required from both a functional kinocilium and the PCP proteins for complete polarization in this tissue.

## PCP is intact in the *bpck* mice

To clarify the potential involvement of meckelin with PCP signaling, PCP-mediated cellular polarization was analyzed in the *bpck* model by examining polarity of basal feet in P1 mouse tracheal tissue. Basal feet are dense appendages of the basal body of motile cilia that form connections to the apical cytoskeleton (61). PCP regulates synchronous orientation of basal bodies of motile cilia in multiciliated cells, such as those in the airway epithelium, to ensure coordinated ciliary beating to propel fluid in a uniform direction (62–64). We found that the organization of basal feet was maintained in both wild-type and *bpck* littermates (Fig. 4A and B), suggesting that the airway epithelium is properly polarized in the *bpck* mutant.

To further confirm that PCP signaling is intact in the *bpck* mouse, we analyzed a different tissue and assayed the asymmetric segregation of core PCP proteins to the apical adherens junctions. Here, we examined the asymmetric localization of the core PCP protein Vangl1 to the medial edge of P1 *bpck* OC hair cells as a robust demonstration of planar polarization of these sensory cells. In agreement with our observation of largely uniform sensory sterocilia alignment in the OC of the *bpck* mouse inner ear, medial localization of Vangl1 was retained in *bpck* OC hair cells and was indistinguishable from wild-type littermates (Fig. 4C and D). This demonstrated that tissue planar polarization is intact in the *bpck* mouse and argues against a clear role for meckelin in PCP signaling. While the loss of meckelin causes the 'PCP-like' phenotype of disorganized stereociliary bundles, the defect is more likely due to the role of the kinocilium in this process.

## Meckelin loss leads to upregulation of canonical Wnt signaling in *bpck* cystic tubules

As a relationship between dysregulation of canonical Wnt and PCP signaling in PKD and the ciliopathies has been proposed, we investigated the levels of canonical Wnt signaling in the *bpck* mouse to determine whether this pathway was defective (38,65–71). Transcriptional dysregulation of Wnt signaling was first examined in P1 whole kidney tissue using a $RT^2$ Profiler real-time PCR array (SABiosciences) that assays 84 Wnt targets. Most targets were upregulated, with 12 transcripts significantly upregulated >2-fold in mutant compared with wild-type kidneys (Fig. 5A, Table 1). Four of these genes are direct targets of Wnt transcription factors: *Ccnd1* (cyclin D1) (72,73), *Fn* (fibronectin) (74), *Myc* (74,75) and *Ppard* (peroxisome proliferation-activated receptor delta) (73). These results indicate that Wnt signaling is globally upregulated in meckelin negative kidneys.

To determine in which part of the kidney Wnt signaling was upregulated, we performed X-gal (5-bromo-4-chloro-indolyl-β-D-galactopyranoside) staining in TOPGAL;*bpck* and wild-type kidneys. The TOPGAL transgenic mouse contains three multimerized TCF/LEF consensus-binding sites with a minimal c-Fos promoter controlling expression of *LacZ* in a β-catenin responsive manner (76). P1 wild-type kidneys showed a low level of staining with the majority of signal in the nephrogenic zone (Fig. 5B), consistent with a role of Wnt in normal nephron development. In *bpck* kidneys, the overall staining intensity was greater than in wild-types (Fig. 5C) with the strongest signal occurring in the epithelial cells surrounding the dilated tubules (Fig. 5D). Elevated levels of Wnt signaling were maintained in P14 *bpck* cyst linings compared with the surrounding interstitum (Fig. 5E), indicating that upregulation of Wnt is specifically associated with cystogenesis in these animals.

To further investigate the consequences of elevated Wnt activity to cyst development, we examined levels of proliferation in P1 kidney tissue in collecting ducts, the most affected kidney segment in the *bpck* mouse model (Fig. 1F and G). Elevated levels of proliferation were detected in *bpck* collecting duct cells compared with wild-type littermate controls (Fig. 5F–G). This elevated proliferation is observed at the same time point where elevated levels of Wnt signaling

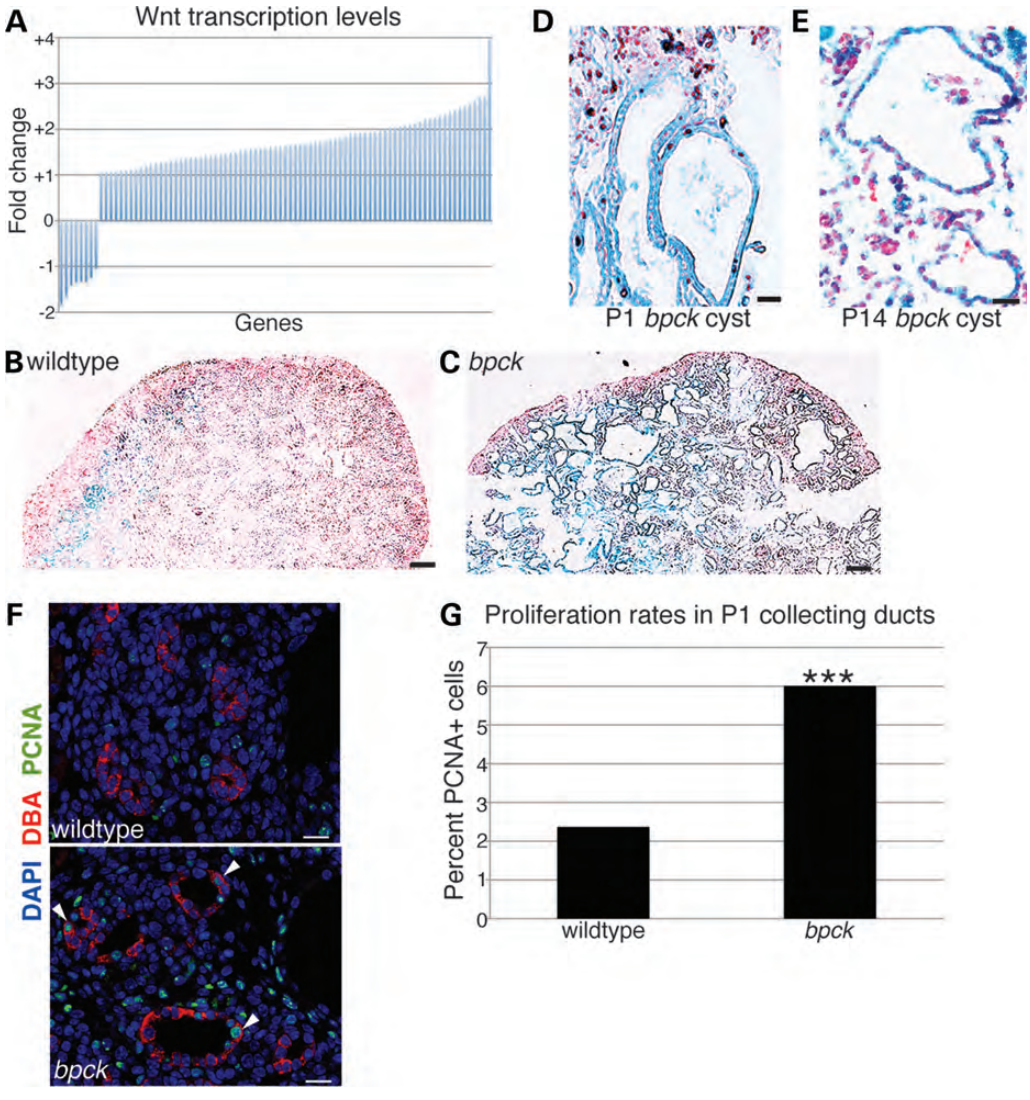


**Figure 5.** Wnt transcription is upregulated in P1 *bpck* kidneys. (**A**) Fold change of Wnt responsive transcripts in *bpck* kidney compared with the wild-type based on RT$^2$ Profiler Array analysis. Image of (**B**) TOPGAL;wild-type and (**C**) TOPGAL;*bpck* kidney after X-gal staining indicating regions of Wnt transcriptional activation (scale bar = 100 μm). Higher resolution images of (**D**) P1 and (**E**) P14 TOPGAL;*bpck* kidney cysts (scale bar = 20 μm). (**F**) P1 outbred wild-type and bpck kidney tissue labeled with biotinylated-DBA (collecting ducts) and PCNA to determine levels of proliferation in the collecting ducts. Arrowheads indicate *PCNA* positive proliferating cells. Scale bar = 20 μm. (**G**) Quantitation of (F). Statistics was based on a two-tailed Fisher's exact test. ($^{***}P \leq 0.0001$; $n = 1108$ wild-type, 1019 *bpck* cells; $n = 167$ wild-type, 102 *bpck* collecting duct tubules).

were present (Fig. 5F–G), indicating that increased Wnt signaling activity may be linked to an increase in proliferation in *bpck* kidney tubules.

## Meckelin levels can influence normal canonical Wnt signaling

To further investigate the level of Wnt deregulation with meckelin removal, we examined Wnt upregulation in affected *bpck* retinal and cochlea tissue by examining levels of nuclear β-catenin. However, in P17 retinal sections from wild-type or *bpck* mice, we did not find a clear difference in β-catenin levels, and limited nuclear β-catenin (data not shown). Also, while nuclear β-catenin was observed in OHCs and supporting cells in the OC, there was not a significant difference between *bpck* and wild-type mice (wild-type = 16.7%, *bpck* = 15.0%, $P = 0.63$), suggesting that abnormal Wnt levels do not contribute to these phenotypes (data not shown).

We further investigated the general requirement of meckelin for Wnt signaling by examining Wnt levels in isolated *bpck* cells and cells with exogenous *TMEM67* expression. Immunofluorescence (IF) labeling of *bpck* mouse embryonic fibroblasts (MEFs) showed increased levels of nuclear β-catenin compared with heterozygous littermate controls (Fig. 6A and B). This was confirmed and shown to affect both nuclear and membrane fractions by western analysis of subcellular fractions (Fig. 6C). To further elucidate the role of *TMEM67* in canonical Wnt signaling, we performed reporter assays employing a β-catenin-responsive TCF/LEF-1 luciferase reporter plasmid in HEK293T cells. Upon induction of Wnt activity with exogenous expression of the canonical pathway components *DVL2* (Dishevelled-2) or *CTNNB1* (β-catenin),

**Table 1.** Wnt transcript fold changes in P1 *bpck* kidneys

| Gene | Description | Fold change | *P*-value |
|---|---|---|---|
| *Abcb1a* | ATP-binding cassette | 2.31 | 0.0246 |
| *Ccnd1* | Cyclin D1 | 2.22 | 0.000468 |
| *Cd44* | CD44 antigen | 2.39 | 0.0137 |
| *Ctgf* | Connective tissue factor | 3.98 | 0.000211 |
| *Egfr* | Epidermal growth factor receptor | 2.28 | 0.0141 |
| *Fn1* | Fibronectin 1 | 2.1 | 0.0383 |
| *Irs1* | Insulin receptor substrate 1 | 2.4 | 0.00386 |
| *Klf5* | Kruppel-like factor 5 | 2.7 | 0.0206 |
| *Myc* | Myelocytomatosis oncogene | 2.11 | 0.0186 |
| *Pdgfra* | Platelet-derived growth factor receptor alpha | 2.48 | 0.0118 |
| *Ppard* | Peroxisome proliferator activator receptor delta | 2.09 | 0.000015 |
| *Tgfb3* | Transforming growth factor beta 3 | 2.16 | 0.00211 |

Statistics are based on Student's *t*-test. $n = 3$ wild-type, 3 *bpck* mice.

Wnt signaling was induced in these cells. However, in the presence of exogenously expressed *TMEM67*, Wnt activity was significantly decreased when stimulated with β-catenin (Fig. 6D). *TMEM67* expression also decreased Wnt activity after stimulation with the upstream modulator of Wnt signaling, DVL2, although this did not reach statistical significance (Fig. 6D). The overall expression of the individual components, and the reduction in Wnt signaling by stimulation with both DVL2 and β-catenin is consistent with a role for meckelin as a negative regulator of Wnt activity and suggests a direct role for the protein in modulating Wnt signaling in kidney epithelial cells as well as in MEFs. In addition, enhanced Wnt signaling does not appear to be associated with some other phenotypes observed in the *bpck* mouse where proliferation may be less evident.

### Zebrafish *tmem67* depletion leads to ciliopathy and CE phenotypes

To gain further insight into conserved roles of meckelin in cilia functionality and cilia-related signaling events, we turned to zebrafish as a model system. We identified one zebrafish *tmem67* ortholog (ENSDARG00000076752). The resultant protein has 982 amino acids and is 58% identical and 74.9% similar to the human protein, based on ClustalW Alignment (Supplementary Material, Fig. S2). To examine potential functions of meckelin during zebrafish development, phenotypes were examined after transient protein depletion by morpholino injection at ∼48 hpf. Morphants developed ciliopathy phenotypes, such as hydrocephalus, body curvature and bilateral pronephric cysts, consistent with other ciliopathy zebrafish models (Fig. 7A–D) (17,69–71,77,78). Two different morpholinos were used to target *tmem67*, a splice blocking morpholino (*tmem67* sp-MO) and a translation blocking morpholino (*tmem67* ATG-MO). Both produced dose-dependent phenotypes, indicating morpholino specificity, with the *tmem67* sp-MO being more potent (Fig. 7E and F, Supplementary Material, Table S2). For this reason, the sp-MO was used for all other experiments, unless indicated. The sp-MO led to complete degradation of mRNA, likely through nonsense mediated decay (Supplementary Material, Fig. S3A). Rescue of these ciliopathy phenotypes by overexpression of human *TMEM67* was attempted; however, injection of even very small amounts of RNA led to the development of similar phenotypes (data not shown), making phenotypic rescue challenging and suggesting that these zebrafish ciliopathy phenotypes are highly sensitive to the amount of functional meckelin present.

We next used the zebrafish model to examine the role of meckelin in cilia maintenance by examining olfactory and lateral line cilia. Cilia organization and length in the olfactory placode and anterior and posterior lateral lines were normal in ∼48 hpf morphants (Supplementary Material, Fig. S3B–D). These data suggest that depletion of zebrafish meckelin levels leads to mild ciliopathy phenotypes; however, the structure of cilia was intact in the examined tissues, similar to the data from the *bpck* mouse.

CE has previously been used as a read-out of functional levels of PCP signaling during zebrafish gastrulation and segmentation, a directional tissue remodeling process that is severely disrupted in many PCP mutants (67–69,77,79–83). Several ciliopathy zebrafish models also display defective CE, suggesting a potential role for these genes in PCP events (67,69,77), although our rodent data did not indicate that meckelin was necessary for PCP-mediated planar polarization (Fig. 4). We investigated if meckelin removal in zebrafish also leads to 'PCP-like' phenotypes by examining CE events. For these studies, meckelin was depleted using the ATG-MO in 7–8 somite-staged embryos. The angle of embryonic tissue elongation (TE) spread around the yolk was measured to assess CE defects. Morphants with a TE angle greater than 65 degrees were defined as having defective TE (Fig. 8A and B). Injection of increasing amounts of morpholino led to a dose-dependent increase in affected TE morphants that could be rescued by overexpression of *TMEM67* RNA, suggesting that *tmem67* is involved in TE during zebrafish development (Fig. 8C and D and Supplementary Material, Table S3). This rescue is in contrast to the effect observed with overexpression of *TMEM67* for the ciliopathy phenotypes (Fig. 7), suggesting that the latter phenotype may be more sensitive to absolute levels of functional meckelin and that the CE and ciliopathy phenotypes may be associated with different functions of meckelin. As an additional assessment of CE, somite length and width measurements were taken after staining the same morphants with *myoD* and *krox20* riboprobes to label the somites and hindbrain, respectively (Fig. 8E and F) (67,83). This analysis confirmed that targeting *tmem67* leads to defective CE events.

### Ciliary defects in zebrafish *tmem67* and *vangl2* morphants

We describe above the 'PCP-like' phenotypes of hair cell misorientation in the *bpck* OC and CE defects in *tmem67* morphants. However, we found intact planar polarity in the *bpck* mouse, suggesting that PCP signaling is functional with meckelin removal. Consequently, we first examined maintenance of planar polarity in the *tmem67* morphants by comparing to phenotypes induced by targeting the core PCP protein Vangl2. Depletion of zebrafish Vangl2 levels using a translation blocking morpholino (83) led to the development of the ciliary phenotypes of body curvature, cysts and hydrocephalus in a similar

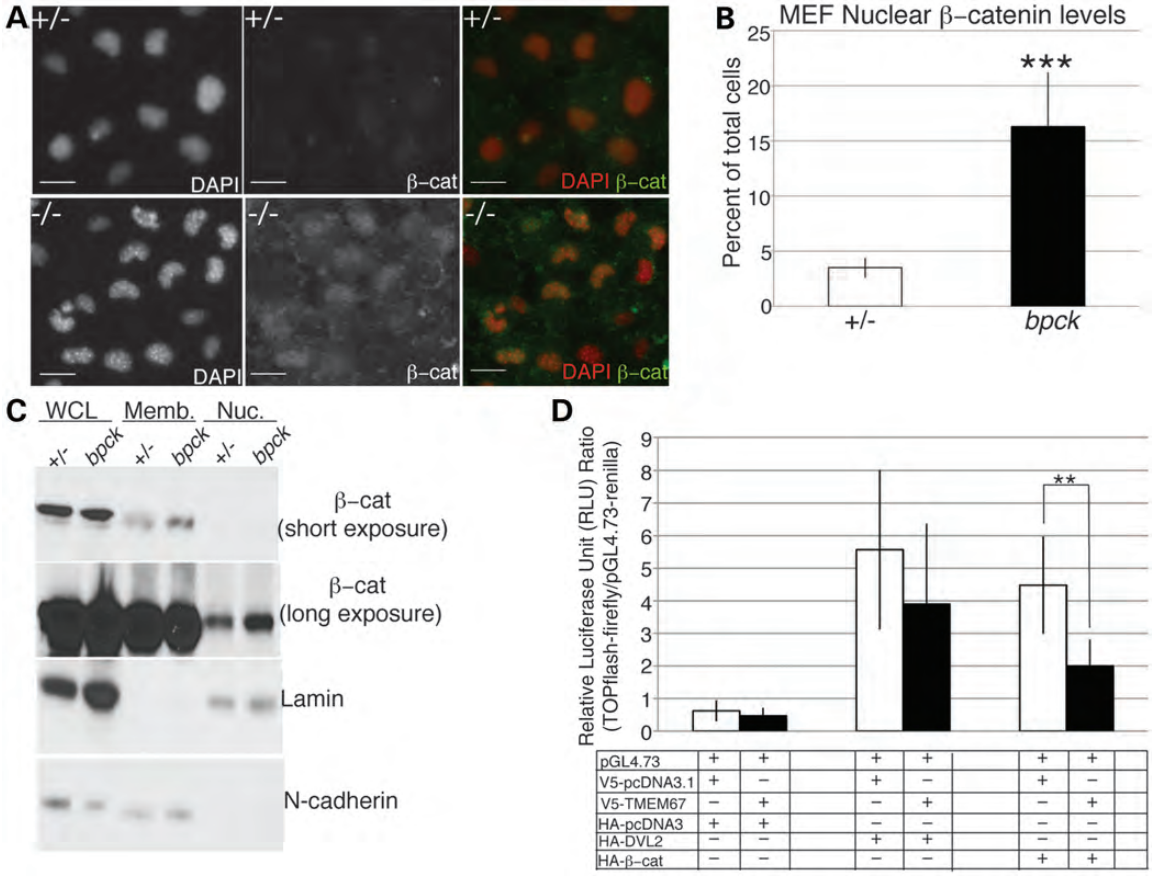


**Figure 6.** Meckelin regulation of canonical Wnt signaling. (**A**) IF analysis of β-catenin localization in heterozygous (+/−) and homozygous (−/−), *bpck*, MEFs. Scale bar = 10 μm. (**B**) Quantitation of nuclear β-catenin levels in MEFs. Data are combined from two representative experiments. ($n = 3336$ +/− cells, 2802 *bpck* cells). Statistics are based on Chi-squared analysis ($^{***}P \leq 0.0001$). (**C**) Western blot displaying levels of β-catenin from subcellular MEF fractionation, showing increased levels in *bpck* membrane and nuclear fractions. Lamin and N-cadherin were used as loading controls. WCL, whole cell lysate; Memb., membrane fraction; Nuc., nuclear fraction. (**D**) β-Catenin responsive luciferase reporter assay (TOPflash) data from HEK293T cells transiently transfected (48 h) with various cDNA constructs: Wnt signaling reporter (firefly luciferase, TOPflash), transfection control (renilla luciferase, pGL4.73), control plasmid (V5 epitope tag, V5-pcDNA3.1(+)), epitope tagged human *TMEM67* cDNA plasmid (V5-*TMEM67*[pcDNA3.1(+)]), control plasmid (HA epitope tag, HA-pcDNA3.1(+)), epitope-tagged human *DVL2* cDNA (HA-*DVL2* [pcDNA3.1(+)]) and epitope-tagged *CTNNB1* cDNA (HA-β-cat [pcDNA3.1(+)]). Data were collected from two independent experiments. Each condition tested was prepared in triplicate for each experiment, and luciferase activity measured independently. Luciferase activity is reported as a ratio, TOPflash/renilla luciferase RLUs. Statistics were based on Student's *t*-test ($^{**}P < 0.01$).

manner to *tmem67* morphants (Fig. 9A). The pronephric duct was also dilated in maternal zygotic (MZ) *vangl2* mutants (84), supporting the specificity of our *vangl2* morphant data. We attempted to examine planar polarity in *tmem67* morphants by orientation of basal feet in the pronephric duct, as performed in *bpck* tracheal tissues; however, this proved to be technically challenging. As a surrogate for this analysis, we examined a downstream consequence of basal feet orientation in the pronephric duct: pronephric cilia beat frequency. *MZvangl2* mutants have disorganized multiciliated pronephric duct cilia (84), and our *vangl2* morphants had a significantly lower pronephric cilia beat frequency than injected control morphants (Fig. 9B and C, Supplementary Material, Movies S1 and S3). Cilia beat frequency was also decreased in *tmem67* morphants compared with controls (Fig. 9B and C, Supplementary Material, Movie S2). However, *vangl2* morphants had a significantly lower beat frequency than *tmem67* morphants and displayed disorganized cilia with no clear coordinated movements (Supplementary Material, Movie S3), which was not observed in *tmem67* morphants (Fig. 9C, Supplementary Material, Movie S2). Consequently, while *tmem67* morphants display cilia beat frequency defects, they are significantly milder than that observed in the *vangl2* morphants and pronephric cilia do not display a dramatic organizational defect as seen in the pronephric duct of *vangl2* morphants. This effect is similar to that observed in the OC of the *bpck* mouse, where the 'PCP-like' defect is much milder than that observed in core PCP mutants. Together, these data provide evidence that although the phenotypes in the *tmem67* and *vangl2* morphants are similar, they appear to result from different mechanisms further showing that planar polarity is intact with meckelin depletion.

## DISCUSSION

In these studies, we have more fully characterized the phenotypes associated with meckelin loss/depletion using the *bpck* mouse model and zebrafish *tmem67* morphants. In the *bpck* mouse, we detected mild tubule dilations as early as E16.5, with mortality and kidney disease severity increased in

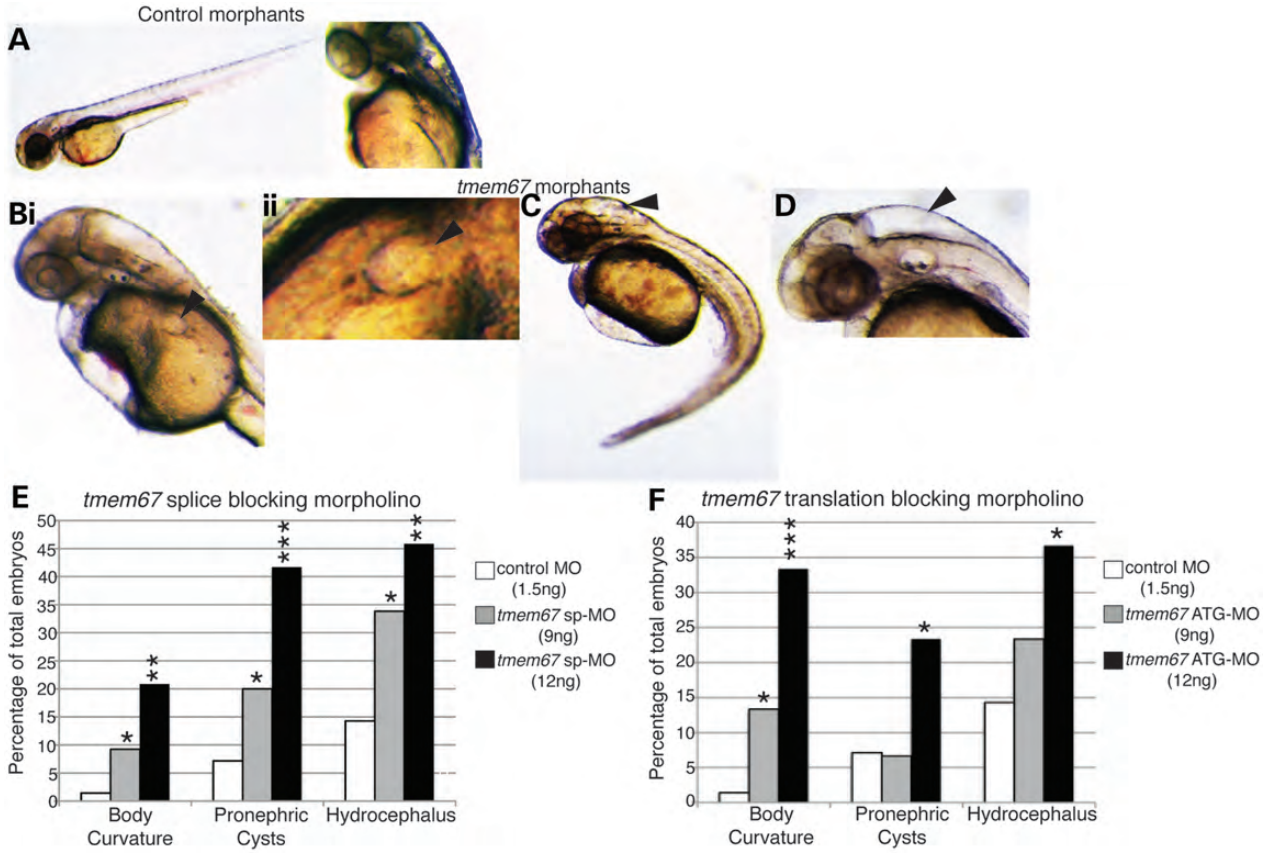


**Figure 7.** Zebrafish meckelin depletion leads to ciliopathy phenotypes. Studies of (**A**) control and (**B**–**D**) morphant zebrafish at ∼48 hpf. (Bi–ii) Representative images of zebrafish morphants with bilateral pronephric cysts, (C) body curvature and (C, D) hydrocephalus. Arrows indicate affected region (B–D). Quantitation of (**E**) *tmem67* splice blocking and (**F**) translation blocking morpholino phenotypes. Between 30 and 80 embryos were examined for each condition (Supplementary Material, Table S2). Statistics are based on Chi-squared analysis and compared with control injected embryos (***$P \leq 0.0001$, **$P < 0.01$, *$P < 0.05$).

C57BL6/J inbred animals, similar to the recently described *Tmem67*$^{-/-}$ mouse (7). These mice also exhibited defects in cilia function, as seen by retinal degeneration and tissue disorganization in the eye, due to a non-functional connecting cilium [Fig. 2, Supplementary Material, Fig. S1; (33,85)]. Novel cochlea defects were also described (Fig. 3) with mild rotational defects of the stereociliary bundles and absence of kinocilia. In *tmem67* zebrafish morphants, pronephric cysts and hydrocephalus were found at a higher level in *tmem67* zebrafish morphants than previously described (55), but in contrast to the previous study, only these phenotypes and body curvature (but not otic, eye defects and cardiac edema) were found to be significant. However, less than half of the animals were affected suggesting that in zebrafish, as in *C. elegans*, depletion of additional ciliopathy genes may be necessary to cause strong, highly penetrant cilia-related phenotypes (9,10,86).

The data described here and in previous studies of rodent models and MKS3 human and mouse cells reveal a complex set of ciliary defects that vary between cell types and tissues. Previous data in kidney cysts showed that cilia formed but were longer than the wild-type and had numerical defects, in contrast to the absence of flagella in the rat sperm (7,33,51). Connecting cilia in MKS3 rodent retinas appeared structurally normal, but in the mouse were unable to transport rhodopsin, transducin or arrestin to the outer segment [Fig. 2, Supplementary Material, Fig. S1; (33,85)]. A similar ciliary trafficking defect was observed in isolated MEFs, where Arl13b and adenylyl cyclase III (AC3) transport to the primary cilium was reduced but Smoothened trafficking unperturbed (7). In our study, a high percentage of sensory hair cells in the cochlea were detected without a kinocilium in *bpck* animals at P1, which we propose occurs due to earlier re-absorption of the kinocilium, which occurs normally at approximately P10 after patterning of the stereocilia bundles is complete, likely from being non-functional (Fig. 3) (87). Evaluation of basal body docking in multiciliated respiratory cells in the *bpck* trachea showed no defective docking (Fig. 2), despite earlier studies suggesting that this process was defective in meckelin-depleted cells (34,55). Clear structural and numerical defects in cilia were also not detected in several ciliated tissues in *tmem67* zebrafish morphants (Supplementary Material, Fig. S3), although these animals developed ciliopathy phenotypes. These data are consistent with the defect in MKS3 only rarely being associated with failure to form cilia (33), but more typically due to abnormal trafficking of a subset proteins on to the cilium, linked with a role for meckelin as part of a membrane protein filter at the transition zone (7).

The role of Wnt signaling in ciliopathies and PKD has been controversial. Canonical Wnt is involved in metanepehric mesenchyme induction and cell proliferation during branching

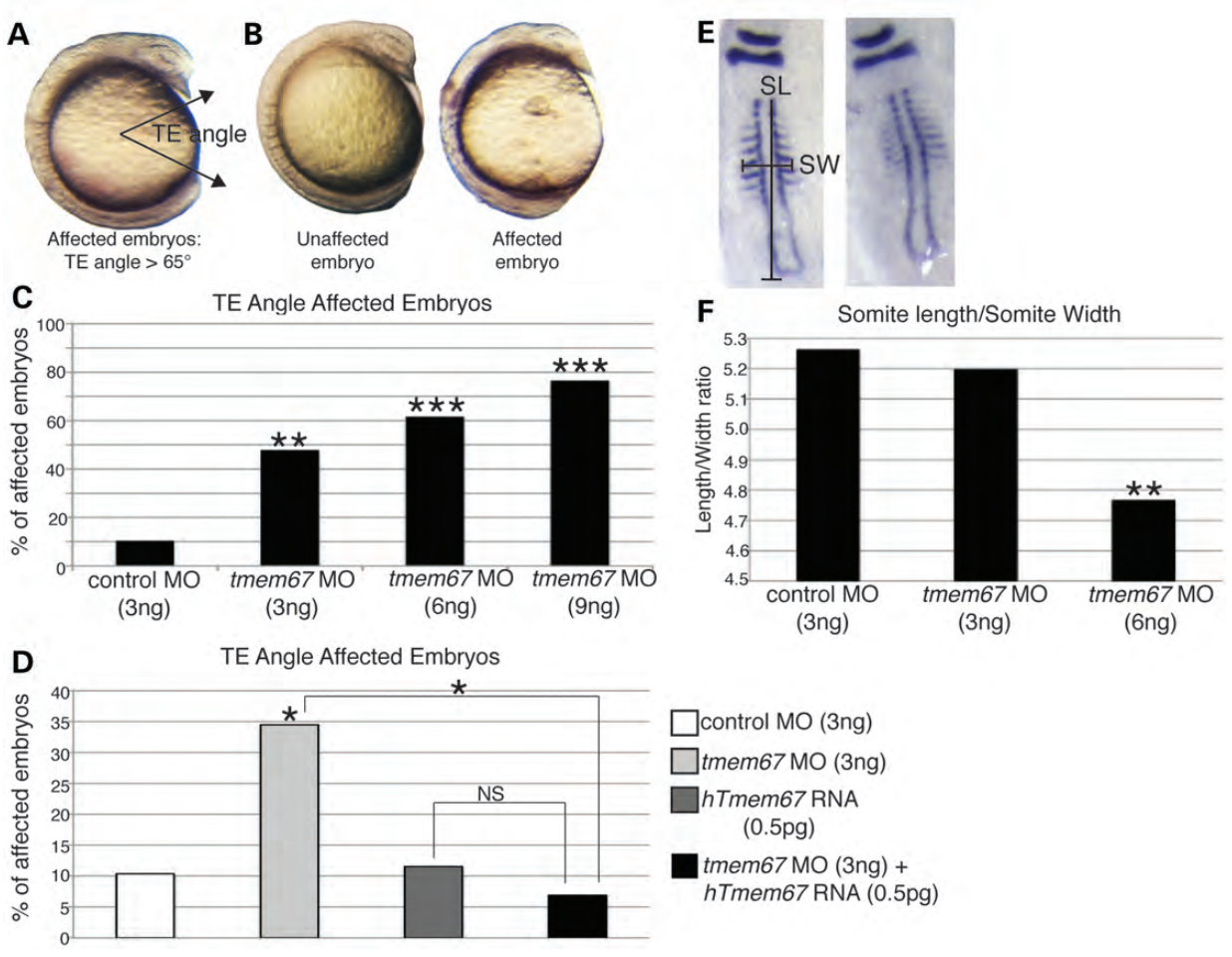


**Figure 8.** 'PCP-like' CE phenotypes occur with meckelin depletion in zebrafish morphants. All TE analysis was performed in 7–8 somite-staged embryos. (**A**) Zebrafish embryo with TE angle indicated; affected embryos had TE angles greater than 65°. (**B**) Representative images of TE unaffected and affected morphants. (**C**) Quantitation of TE defects with dose escalation of *tmem67* ATG-MO and (**D**) rescue of TE phenotype with human *TMEM67* RNA injection. Approximately 25–95 embryos were examined for each condition (Supplementary Material, Table S3). Statistics are based on Chi-Squared analysis compared with control-MO or MO + RNA injected embryos, as indicated (***$P \leq 0.0001$, **$P < 0.01$, *$P < 0.05$). (**E**) Representative 7–8 somite-staged embryos stained with *myoD* (somites) and *krox20* (hindbrain) riboprobes to analyze somite length (SL) and somite width (SW) ratios. Images are dorsal views of flatten embryos with the yolk removed. (**F**) Quantitation of somite length to width defects with *tmem67* ATG-MO. Control morphants $n = 19$; *tmem67* morphants (3 ng) $n = 45$; *tmem67* morphant (6 ng) $n = 44$. Statistics are based on Student's *t*-test (**$P < 0.01$).

morphogenesis in early kidney development and may become reactivated in PKD to repair damaged tissue (88–91). In human NPHP2, a switch from PCP signaling to canonical Wnt activation was suggested as the pathogenic principle (78). This model remains a strong paradigm for the contribution of canonical Wnt signaling to renal cystogenesis. Here, we demonstrate that the canonical pathway is upregulated in P1 and P14 *bpck* kidneys with canonical Wnt activity concentrated in cyst linings, with enhanced proliferation also detected in P1 *bpck* kidney tissue. Wnt activity was not elevated in cochlear or retinal *bpck* cells, where the phenotype is unlikely to be caused by heightened proliferation levels. This is consistent with canonical Wnt signaling playing an active role in promoting or accelerating cystogenesis by enhancing proliferation, similar to other PKD models (36,55,67,69,92,93). Our data suggest that meckelin restrains canonical Wnt activity, which could not be rescued by overexpression of β-catenin. The identification of meckelin in the MKS-B9 protein module at the transition zone (TZ) suggests that meckelin may exert this observed negative regulatory function by a general role as a gating factor at the TZ to control trafficking of a specific set of signaling factors to and from the ciliary compartment. In support of this, lack of a functional cilium, such as with meckelin removal, may disrupt the sequestration of canonical Wnt components, leading to increased transcriptional activity and cellular proliferation (36,39). More specifically, meckelin may act as a membrane anchor to spatially organize the β-catenin destruction complex at the ciliary base (38). Lack of meckelin may disrupt formation of this complex, allowing β-catenin to escape degradation and remain transcriptionally active (39,94). This is supported by our finding of elevated levels of β-catenin in *bpck* kidney epithelial cells and MEFs.

Conversely, the non-canonical Wnt pathway, PCP, is proposed to be downregulated in PKD (2) and to directly contribute to cystogenesis (95) and other ciliopathy phenotypes; however, this involvement is controversial. Loss of meckelin in the *bpck* mouse caused the 'PCP-like' phenotype of

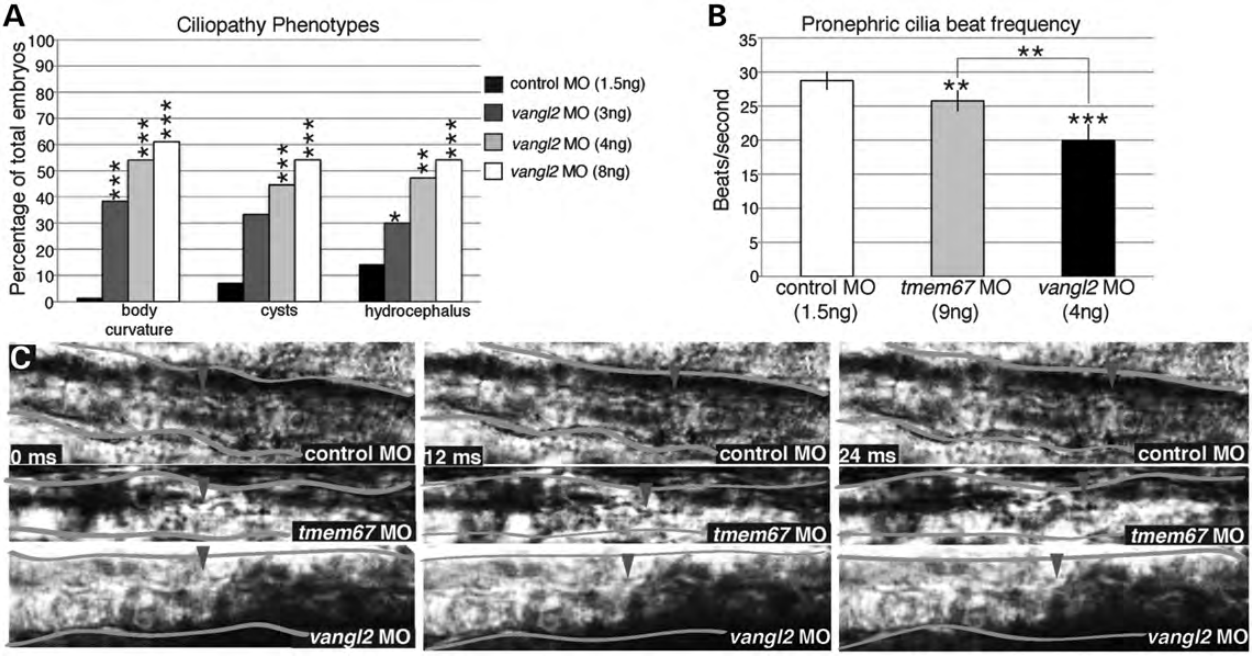


**Figure 9.** Comparison of ciliary phenotypes in zebrafish morphants of *tmem67* and the core PCP gene *vangl2*. (**A**) Quantitation of ciliopathy phenotypes after *vangl2* depletion in ∼48 hpf embryos. Approximately 50–80 embryos were examined for each condition. Statistics are based on Chi-squared analysis ($^{***}P \leq 0.0001$, $^{**}P < 0.01$, $^{*}P < 0.05$). (**B**) Quantitation of pronephric cilia beat frequency in ∼48 hpf morphants. Data are from two representative experiments, with 4–6 embryos examined for each condition. Statistics are based on Student's *t*-test ($^{***}P \leq 0.0001$, $^{**}P < 0.01$). (**C**) Still frames of ciliary waves from Supplementary Material, Movies S1–S3. Arrowheads indicate the progression of a single ciliary wave throughout the examined time span. The pronephric duct is outlined.

stereocilia misalignment in the OC with hair cells displaying significant rotational defects away from the lateral edge of the OC (Fig. 3). However, hair cells in core PCP mouse mutants, such as *Vangl2/Stbm* (Looptail), rotate up to 100 to 210 degrees from the lateral edge of the OC (57), while *bpck* hair cells rotated a maximum of 51 to 60 degrees. The phenotype of extra rows of hair cells seen in PCP mutants was also not significantly elevated in the *bpck* mice. A milder rotational phenotype, similar to that in the *bpck*, was observed in BBS (56) and structural cilia protein mutant models, such as in conditional *Ift88* and *Kif3a* mice (43,59). It is thought that input from both the core PCP pathway and the kinocilium and associated proteins are necessary for complete polarization of hair cells, implying interaction between these pathways (43,59). Given the milder stereociliary phenotype detected in the *bpck* mouse, the stereocilia misalignment seems more likely associated with loss of kinocilium function than defective PCP signaling. This interpretation is supported by the failure to detect direct planar polarization defects in *bpck* tissues when well-established vertebrate PCP-dependent processes, such as coordinated polarization of motile cilia in airway epithelial cells and asymmetric protein localization of Vang1 in the OC, were examined. Although we cannot rule out PCP defects in other tissues or stringently conclude that all of PCP signaling is functional by examining a few phenotypes, these data support a functional PCP pathway in the *bpck* mouse model. Furthermore, no renal cysts have been documented in mouse *Vangl2/Stbm* mutants and only *Fat4* and *Nphp2*/*Inversin* PCP-related mouse mutants develop PKD (48,96), perhaps because of their additional roles in the development of functional cilia or in directional tissue morphogenesis, although it is unclear how closely renal cystogenesis has been examined in many core PCP mutants.

'PCP-like', CE defects were also observed with meckelin depletion in zebrafish morphants, although our analysis also suggested that planar polarity, and consequently PCP signaling, was intact in *tmem67* morphants due to coordinated, synchronized ciliary beating compared with that in *vangl2* morphants. Defective CE has been used as a functional readout of PCP signaling in ciliopathy models and is observed in core PCP zebrafish mutant models (67,78,82,83). However, CE is a complex process that involves many pathways and, therefore, CE phenotypes do not necessarily equate with disrupted PCP signaling (35,97–99). Although the PCP pathway is a major player in CE, its role appears to be more permissive than instructive and involves input from multiple different signaling pathways and molecules including: Wnt, Nodal, BMP (bone morphogenic protein) and FGF (fibroblast growth factor), Stat3 and G protein coupled-receptor pathways (97–99). Additionally, transcription factors such as Brachyury and Snail, adhesion molecules, extracellular matrix components, cytoskeleton factors, various receptors, axon guidance proteins and components involved in endocytosis have all been implicated in maintaining proper CE, demonstrating the complexity of events involved in this process (99).

Instead of being directly involved in PCP-mediated CE, we propose that meckelin plays a role in CE through cilia and centrosome functioning. The centrosome is proposed to detect polarizing information in a three-dimensional sense in the cell and consequently may function as a mediator of polarity on the cellular level (35). We have previously shown that meckelin removal causes a multiple centrosome phenotype,

which could cause defects in polarized cell migration and oriented cell division, both essential processes for CE at the level of the centrosome and thus may be responsible for CE defects mediated by meckelin removal rather than a direct involvement of meckelin in PCP-mediated CE (33,97,99).

This study indicates that no strong defects in cilia formation, basal body docking or PCP dysfunction occur with meckelin removal. Instead, our data support the hypothesis that defects associated with *TMEM67* mutation are likely due to only partially functional cilia in a range of different tissues. Aberrations were observed in canonical Wnt signaling, which may be related to cilia-dependence of this pathway. Therefore, we reaffirm a role of meckelin at the cilia/centrosome compartment and propose that defects in protein functioning at this level are largely responsible for the phenotypes observed in MKS3.

## MATERIALS AND METHODS

### Mice

Mice were housed at the Mayo Clinic Mouse Facility according to NIH and Institutional Animal Care and Use Committee (IACUC, Mayo Clinic, Rochester, MN, USA) guidelines. *bpck* mice were obtained from Jackson Laboratories (Bar Harbor, ME, USA) and were maintained on a C57BL6/J background. Inbred animals were backcrossed 10 generations and outbred mice were in mixed C57BL6/J;B6C3FeF1/J*a/a* or C57BL6/J;LacZ backgrounds. TOPGAL mice were kindly provided by John Hawse at the Mayo Clinic. *bpck* and LacZ mice were genotyped using the following primers: 5′-GCACTATGTTAAAAGATCCAG-3′ and 5′-ATTCTGCTGAACACCCCACAG-3′ (wild-type allele), 5′-TGTCAAACCACCCTCTAAGCCTG-3′ and 5′-CAGCCTCACATCACTTTACCTAACG-3′ (*bpck* allele), 5′-ATCCTCTGCATGGTCAGGTC-3′, 5′-CGTGGCCTGATTCATTCC-3′, 5′-CAAATGTTGCTTGTCTGGTG-3′ and 5′-GTCAGTCGAGTGCACAGTTT-3′ (*LacZ* alleles). Cystic tubule measurements were performed using the ImageJ software.

### Zebrafish

Zebrafish were housed at the Mayo Clinic Zebrafish Core Facility according to the NIH and IACUC guidelines. Wild-type Tu or Segrest lines were utilized. Staging was performed by counting somites or by other standard protocols (79).

### X-gal staining

Whole mouse kidneys were dissected and fixed in whole mount fix (0.2% glutaraldehyde, 5 mM EGTA and 2 mM $MgCl_2$ in 0.1 M phosphate buffer) on ice for 1 h. Kidneys were washed 3 × 30 min in detergent rinse (0.02% Igepal, 0.01% sodium deoxycholate and 2 mM $MgCl_2$ in 0.1 M phosphate buffer). Tissue was stained overnight at 37°C in the dark in X-gal staining solution (1 mg/ml X-gal 0.02% Igepal, 0.01% sodium deoxycholate, 5 mM potassium ferricyanide, 5 mM potassium ferrocyanide and 2 mM $MgCl_2$ in 0.1 M phosphate buffer). Kidneys were then washed in PBS and stored in 4% paraformaldehyde (PFA; Electron Microscopy Sciences; Hatfield, PA, USA). Kidneys were embedded in paraffin and sectioned. Slides were de-waxed, rehydrated, counter-stained with Nuclear Fast red and preserved with Vectashield (Vector Labs; Burlingame, CA, USA).

### Electron microscopy

For SEM, inner ears were dissected from mice and fixed in 4% PFA for at least 24 h. Cochleae were dissected from fixed tissue, and the OC was isolated and fixed at least overnight in 4% PFA and post-fixed in Trump's fixative (4% PFA, 1% glutaraldehyde). The remaining process was carried out using standard procedures by the EM core facility at the Mayo Clinic, as previously described (33). For TEM, the samples were fixed in Trump's fixative for 2–3 h, washed in 0.1 M phosphate buffer 3 × 15 min, post-fixed in 1% osmium tetroxide in 0.1 M phosphate buffer for 1–2 h at room temperature, washed three to five times (10 min each) in distilled water, then En bloc stained with 2% aqueous uranyl acetate for 1 h at room temperature, washed two to three times (5 min each) in distilled water, dehydrated through an ethanol series, embedded in Spurrs resin, sectioned at 80 nm, stained with lead citrate for 3–15 min and examined with a JEOL 1400 electron microscope (JEOL USA, Peabody, MA, USA).

### Zebrafish microinjection

All morpholino and RNA solutions were injected into 1–4 cell embryos in volumes of 3–9 nl at the indicated concentrations. RNA was synthesized from a linearized pcDNA3.1 vector template using the T7 mMESSAGE mMACHINE High Yield Capped RNA Transcription Kit (Ambion, Life Technologies). Morpholinos were manufactured by Gene Tools (Philomath, OR, USA). Unless otherwise noted, morpholinos were designed by Gene Tools using the Oligo Design service. Two morpholinos were used against *tmem67*: a translation blocking morpholino (5′-GATCAGATGACGCTTGATGACGTAT-3′) and a morpholino targeting the intron 8/exon 9 splice acceptor site (5′-AGAACAACTACAGAAGAACAATAAC-3′). The splice blocking morpholino efficacy was tested with primers in exon 7 (5′- AATGTGCTTCCCTGCGAACAGTCTGC-3′) and exon 10 (5′- CCAAGGTAGGTTTGTCCTCCAGTAG-3′). Additional morpholinos were previously tested in published literature against the translation start site of *vangl2* (83). The control morpholino used targets mutated human β-globin and has no target in zebrafish (Gene Tools). TE measurements were performed on printed images using a protractor and compass. Ciliopathy phenotypes were analyzed in a blinded manner. All experiments were repeated three times and with three different dosages of morpholino. Level of control morpholino to use for each experiment was determined by matching death rates between the control and experimental morpholino. RNA levels for the CE rescue experiments were chosen based on levels that did not produce a phenotype when injected alone. All levels of *TMEM67* RNA injected produced ciliopathy phenotypes.

### RNA extraction and cDNA analysis

RNA for morpholino analysis was extracted from ∼5–10 pooled embryos. Embryos were homogenized with needles in

Trizol and RNA was extracted by successive chloroform, isopropyl alcohol extractions. cDNA was synthesized using the Superscript III First Strand Synthesis System with random primers according to the manufacturer instruction (Life Technologies; Grand Island, NY, USA). RNA was extracted from whole mouse kidneys for transcript analysis on the $RT^2$ WNT Signaling Target PCR Array (Mouse) chip from SABiosciences (Valencia, CA, USA). RNA was isolated using a Qiagen RNeasy Mini Kit and cDNA synthesis performed using the $RT^2$ First Strand Kit (SABiosciences). Transcript analysis was performed employing the $RT^2$ WNT Signaling Target PCR Array (Mouse) chip (SABiosciences). Chips were run on a 7900HT Real-Time 384 well PCR machine (Applied Biosystem). Data were analyzed by the ΔΔCt method using the PCR Array Data Analysis Web Portal software (SABiosciences).

## IF labeling

*Cochleae*

OCs were isolated as above and fixed in 4% PFA. OCs were washed three times in buffer T [0.1 M Tris (pH 7.5), 0.15 M NaCl and 0.1%Triton X-100] and then incubated in blocking buffer (buffer T with 10% fetal bovine serum) for 1 h. Samples were incubated overnight in primary antibody diluted in blocking buffer. OCs were then washed with buffer T, incubated in secondary antibody for 1 h and washed again. Whole OCs were mounted in Vectashield (Vector Labs) on slides for analysis. Antibodies used include: rabbit anti-human Vangl1 pAb (Sigma-Aldrich; St Louis, MO, USA), Alexa Fluor-conjugated phallodin [Life Technologies (Molecular Probes)] and Alexa Fluor 488 goat anti-rabbit IgG [Life Technologies (Molecular Probes)]. All samples were visualized on a Zeiss AxioObserver microscope at ×40 magnification (Carl Zeiss).

*Mouse embryonic fibroblasts*

Fibroblasts were prepared from E13.5 embryos. Pregnant females and embryos were euthanized according to IACUC standards and embryos removed and washed briefly in PBS. Embyos were decapitated, eviscerated, diced and trypsinized. Fully trypsinized cells were plated on tissue culture plastic as passage 1. For IF, cells were grown to 90% confluence in DMEM/F12 10% FBS on glass cover slips. Cells were then washed twice with PBS, fixed and permeabilized 5 min with ice-cold methanol. Slides were washed twice in PBS and incubated in 5% BSA in PBS for 1 h. Primary anti-β-catenin antibody (Cell Signaling, 9562) was applied overnight in 1% BSA in PBS. Secondary Alexa Fluor 488 goat anti-rabbit IgG [Life Technologies (Molecular Probes)] was used for 1 h followed by DAPI. Cover slips were washed in PBS and mounted on charged slides using Vectashield H-1000 mounting medium (Vector Labs). Nuclear β-catenin/DAPI co-localization was scored and quantified with ImageJ.

*Mouse kidney tissue*

IF was performed on kidney tissue sections as previously described (33). Primary antibodies used included: biotinylated –LTA and –DBA (1:250, Vector Laboratories), THP (1:200, Santa Cruz Biotechnology Inc.), and PCNA (1:100, Santa Cruz Biotechnology Inc.). Secondary antibodies included: Alexa Fluor conjugated streptavidin, goat anti-rabbit IgG and goat anti-mouse IgG2a [Life Technologies (Molecular Probes)]. Nuclei were counterstained with DAPI (Life Technologies).

All IF samples were imaged using an AxioObserver and Axiovision 4.8 software (Carl Zeiss).

## Statistics

Two-tailed Fisher's exact test was performed as previously described (33). Chi-squared distributions and Student's *t*-test were calculated using Microsoft Excel.

## Whole mount zebrafish *in situ*

Regions of *myoD* and *krox20* were amplified for probe synthesis using the following primer sets: *myoD* (5′-CTTGGACC CCAGGCTTGTTCAC-3′, 5′-GGTAATACGACTCACTATA GGGTTCCGTCTTCTCGTCTGACACG-3′) and *krox20* (5′-T CGCACAGACACAACACATTC-3′, 5′-GGTAATACGACTC ACTATAGGTGGGGTATTTCCTTGGACGC-3′). A T7 promoter was added to the reverse primer for amplification. Riboprobes were created using the Ampliscribe T7 kit with DIG RNA labeling mix (Roche). Zebrafish embryos for analysis were collected at the indicated times, the chorions were removed and embryos were fixed overnight at 4 degrees in 4% PFA. Whole-mount stainings were performed as described (100). Embryos were cleared in 70% glycerol/PBS for imaging.

## Mouse skeletal whole-mount staining

Pregnant females and embryos were euthanized according to IACUC standards. Embryos were dissected and stained as previously described (101).

## Cellular fractionations

For MEF subcellular fractionation, cells were resuspended in a hypotonic solution (10 mM HEPES pH 7.5, 10 mM KCl, 2.5 mM $MgCl_2$) and homogenized. Cells were spun at 600*g* for supernatant (SN1) and pellet (P1) fractionation. SN1 was spun at 22 000*g* for 30 min (SN2). The pellet was resuspended in a solubilization buffer (10 mM Tris–HCl pH 7.5, 500 mM NaCl, 1 mM EDTA, 1% Triton X-100) and centrifuged at 16 000*g* for 30 min. The resulting supernatant (SN3) represented the membrane fraction. Pellet from the original centrifugation (P1) was resuspended in 100 μl of nuclear lysis buffer (50 mM HEPES pH 7.9, 250 mM KCl, 0.1% NP40, 0.1 mM EDTA) and centrifuged at 16 000*g* for 10 min. Supernatant from the final centrifugation represented the nuclear fraction (N1). All buffers were supplemented with protease inhibitors (Roche) and fractionation performed on ice.

## Western blotting

Antibodies for western blotting were diluted in 5% Non-fat dry milk in TBST: β-catenin (Cell signaling 9562S 1:2000), Lamin A/C (Santa Cruz N-18 1:2000), Alpha Tubulin (Sigma T6199, mouse IgG1 1:5000), N-cadherin (Life Technologies 33–3900, and mouse IgG1 1:1000).

### Luciferase assays

HEK293T cells (ATCC) were grown according to the manufacturer's instructions. Cells were plated in six-well plates, and transfected with Polyfect (Qiagen) according to the manufacturer's protocol. The following constructs were transfected into cells: Wnt signaling reporter (firefly luciferase, TOPflash, Millipore), transfection control (renilla luciferase, pGL4.73, Promega), control plasmid (V5 epitope tag, pcDNA3.1(+), Life Technologies), epitope tagged human *TMEM67* cDNA plasmid (N-terminal V5 epitope inserted after the signal peptide, pcDNA3.1(+), Life Technologies), control plasmid (HA epitope tag, pcDNA3.1(+), Life Technologies), epitope-tagged human *DVL2* cDNA (N-terminal HA epitope, pcDNA3.1(+), Life Technologies) and epitope-tagged *CTNNB1* cDNA (N-terminal HA epitope tag, pcDNA3.1(+), Life Technologies). The cell media was replaced 24 h post-transfection, and cells were lysed and prepared for luminescence measurements 48 h post-transfection. The Dual-Luciferase Reporter Assay system (Promega) was used for sample preparation according to the manufacturer's protocol. Sample luminescence was measured using dual automatic injection (Luminometer 20/$20^n$, Turner Biosystems).

### cDNA cloning

pcDNA3.1(+) vectors were modified by insertion of coding sequences for V5- and HA-epitope tags between the *Nhe*I- and *Bam*HI-restriction site. Human cDNAs for *DVL2*, *CTNNB1* and *TMEM67* were amplified by RT–PCR from 293T cell mRNA using gene-specific primers. *DVL2* and *CTNNB1* were cloned into the respective plasmids using *Bam*HI and *Not*I restriction enzymes to generate tagged constructs. For *TMEM67*, a V5-tag was inserted by fusion PCR between the signal peptide sequence and the putative first amino acid of the N-terminal domain and later subcloned into pcDNA3.1(+). The exact primer sequences and cloning strategies are available from the authors upon request.

## SUPPLEMENTARY MATERIAL

Supplementary Material is available at *HMG* online.

## ACKNOWLEDGEMENTS

Scott Gamb in the Mayo EM core provided expertise for the SEM in both zebrafish and mouse models and also helped to examine the mouse retinas by TEM. Trace Christensen in the Mayo EM core performed analysis of basal feet and multiciliated tracheal cells by TEM. Drs Jennifer Westendorf and Megan McGee-Lawrence provided expertise for the bone studies and Dr Samih Nasr aided in histological analysis. Dr Iain Drummond at Harvard University provided his knowledge and expertise in training A.C.L. in techniques and methods to examine ciliopathy phenotypes in zebrafish. Xiaolei Xu, Xueying Lin and Steve Ekker at the Mayo Clinic were also extremely helpful in teaching zebrafish techniques, and providing reagents and advice. Vincent Gattone at Indiana University School of Medicine was helpful in discussion and techniques in regards to the *bpck* mice. John Hawse at Mayo Clinic is thanked for providing the TOPGAL mice.

*Conflict of Interest statement*. None declared.

## FUNDING

This work was supported by the National Institute of Diabetics and Digestive and Kidney Disease grant (DK059597). A.C.L.'s predoctoral studentship is supported by the Zell Family Foundation. The Mayo PKD Translational Center (DK090728) provided support for the zebrafish and mouse studies.

## REFERENCES

1. Badano, J.L., Mitsuma, N., Beales, P.L. and Katsanis, N. (2006) The ciliopathies: an emerging class of human genetic disorders. *Annu. Rev. Genomics Hum. Genet.*, **7**, 125–148.
2. Bisgrove, B.W. and Yost, H.J. (2006) The roles of cilia in developmental disorders and disease. *Development*, **133**, 4131–4143.
3. Fliegauf, M., Benzing, T. and Omran, H. (2007) When cilia go bad: cilia defects and ciliopathies. *Nat. Rev. Mol. Cell Biol.*, **8**, 880–893.
4. Hildebrandt, F., Benzing, T. and Katsanis, N. (2011) Ciliopathies. *N. Engl. J. Med.*, **364**, 1533–1543.
5. Goetz, S.C. and Anderson, K.V. (2010) The primary cilium: a signalling centre during vertebrate development. *Nat. Rev. Genet.*, **11**, 331–344.
6. Harris, P.C. (2007) Genetic complexity in Joubert syndrome and related disorders. *Kidney Int.*, **72**, 1421–1423.
7. Garcia-Gonzalo, F.R., Corbit, K.C., Sirerol-Piquer, M.S., Ramaswami, G., Otto, E.A., Noriega, T.R., Seol, A.D., Robinson, J.F., Bennett, C.L., Josifova, D.J. *et al.* (2011) A transition zone complex regulates mammalian ciliogenesis and ciliary membrane composition. *Nat. Genet.*, **43**, 776–784.
8. Sang, L., Miller, J.J., Corbit, K.C., Giles, R.H., Brauer, M.J., Otto, E.A., Baye, L.M., Wen, X., Scales, S.J., Kwong, M. *et al.* (2011) Mapping the NPHP-JBTS-MKS protein network reveals ciliopathy disease genes and pathways. *Cell*, **145**, 513–528.
9. Williams, C.L., Li, C., Kida, K., Inglis, P.N., Mohan, S., Semenec, L., Bialas, N.J., Stupay, R.M., Chen, N., Blacque, O.E. *et al.* (2011) MKS and NPHP modules cooperate to establish basal body/transition zone membrane associations and ciliary gate function during ciliogenesis. *J. Cell Biol.*, **192**, 1023–1041.
10. Williams, C.L., Masyukova, S.V. and Yoder, B.K. (2010) Normal ciliogenesis requires synergy between the cystic kidney disease genes MKS-3 and NPHP-4. *J. Am. Soc. Nephrol.*, **21**, 782–793.
11. Garcia-Gonzalo, F.R. and Reiter, J.F. (2012) Scoring a backstage pass: mechanisms of ciliogenesis and ciliary access. *J. Cell Biol.*, **197**, 697–709.
12. Czarnecki, P.G. and Shah, J.V. (2012) The ciliary transition zone: from morphology and molecules to medicine. *Trends Cell Biol.*, **22**, 201–210.
13. Davis, E.E. and Katsanis, N. (2012) The ciliopathies: a transitional model into systems biology of human genetic disease. *Curr. Opin. Genet. Dev.*, **22**, 290–303.
14. Alexiev, B.A., Lin, X., Sun, C.C. and Brenner, D.S. (2006) Meckel-Gruber syndrome: pathologic manifestations, minimal diagnostic criteria, and differential diagnosis. *Arch. Pathol. Lab. Med.*, **130**, 1236–1238.
15. Harris, P.C. (2009) 2008 Homer W. Smith Award: insights into the pathogenesis of polycystic kidney disease from gene discovery. *J. Am. Soc. Nephrol.*, **20**, 1188–1198.
16. Kyttala, M., Tallila, J., Salonen, R., Kopra, O., Kohlschmidt, N., Paavola-Sakki, P., Peltonen, L. and Kestila, M. (2006) MKS1, encoding a component of the flagellar apparatus basal body proteome, is mutated in Meckel syndrome. *Nat. Genet.*, **38**, 155–157.
17. Valente, E.M., Logan, C.V., Mougou-Zerelli, S., Lee, J.H., Silhavy, J.L., Brancati, F., Iannicelli, M., Travaglini, L., Romani, S., Illi, B. *et al.* (2010) Mutations in TMEM216 perturb ciliogenesis and cause Joubert, Meckel and related syndromes. *Nat. Genet.*, **42**, 619–625.

18. Smith, U.M., Consugar, M., Tee, L.J., McKee, B.M., Maina, E.N., Whelan, S., Morgan, N.V., Goranson, E., Gissen, P., Lilliquist, S. *et al.* (2006) The transmembrane protein meckelin (MKS3) is mutated in Meckel-Gruber syndrome and the wpk rat. *Nat. Genet.*, **38**, 191–196.
19. Baala, L., Audollent, S., Martinovic, J., Ozilou, C., Babron, M.C., Sivanandamoorthy, S., Saunier, S., Salomon, R., Gonzales, M., Rattenberry, E. *et al.* (2007) Pleiotropic effects of CEP290 (NPHP6) mutations extend to Meckel syndrome. *Am. J. Hum. Genet.*, **81**, 170–179.
20. Delous, M., Baala, L., Salomon, R., Laclef, C., Vierkotten, J., Tory, K., Golzio, C., Lacoste, T., Besse, L., Ozilou, C. *et al.* (2007) The ciliary gene RPGRIP1L is mutated in cerebello-oculo-renal syndrome (Joubert syndrome type B) and Meckel syndrome. *Nat. Genet.*, **39**, 875–881.
21. Tallila, J., Jakkula, E., Peltonen, L., Salonen, R. and Kestila, M. (2008) Identification of CC2D2A as a Meckel syndrome gene adds an important piece to the ciliopathy puzzle. *Am. J. Hum. Genet.*, **82**, 1361–1367.
22. Shaheen, R., Faqeih, E., Seidahmed, M.Z., Sunker, A., Alali, F.E., AlQahtani, K. and Alkuraya, F.S. (2011) A TCTN2 mutation defines a novel Meckel Gruber syndrome locus. *Hum. Mutat.*, **32**, 573–578.
23. Hopp, K., Heyer, C.M., Hommerding, C.J., Henke, S.A., Sundsbak, J.L., Patel, S., Patel, P., Consugar, M.B., Czarnecki, P.G., Gliem, T.J. *et al.* (2011) B9D1 is revealed as a novel Meckel syndrome (MKS) gene by targeted exon-enriched next-generation sequencing and deletion analysis. *Hum. Mol. Genet.*, **20**, 2524–2534.
24. Dowdle, W.E., Robinson, J.F., Kneist, A., Sirerol-Piquer, M.S., Frints, S.G., Corbit, K.C., Zaghloul, N.A., van Lijnschoten, G., Mulders, L., Verver, D.E. *et al.* (2011) Disruption of a ciliary B9 protein complex causes Meckel syndrome. *Am. J. Hum. Genet.*, **89**, 94–110.
25. Bergmann, C., Fliegauf, M., Bruchle, N.O., Frank, V., Olbrich, H., Kirschner, J., Schermer, B., Schmedding, I., Kispert, A., Kranzlin, B. *et al.* (2008) Loss of nephrocystin-3 function can cause embryonic lethality, Meckel-Gruber-like syndrome, situs inversus, and renal-hepatic-pancreatic dysplasia. *Am. J. Hum. Genet.*, **82**, 959–970.
26. Consugar, M.B., Kubly, V.J., Lager, D.J., Hommerding, C.J., Wong, W.C., Bakker, E., Gattone, V.H. 2nd, Torres, V.E., Breuning, M.H. and Harris, P.C. (2007) Molecular diagnostics of Meckel-Gruber syndrome highlights phenotypic differences between MKS1 and MKS3. *Hum. Genet.*, **121**, 591–599.
27. Khaddour, R., Smith, U., Baala, L., Martinovic, J., Clavering, D., Shaffiq, R., Ozilou, C., Cullinane, A., Kyttala, M., Shalev, S. *et al.* (2007) Spectrum of MKS1 and MKS3 mutations in Meckel syndrome: a genotype-phenotype correlation. Mutation in brief #960. Online. *Hum. Mutat.*, **28**, 523–524.
28. Baala, L., Romano, S., Khaddour, R., Saunier, S., Smith, U.M., Audollent, S., Ozilou, C., Faivre, L., Laurent, N., Foliguet, B. *et al.* (2007) The Meckel-Gruber syndrome gene, MKS3, is mutated in Joubert syndrome. *Am. J. Hum. Genet.*, **80**, 186–194.
29. Otto, E.A., Tory, K., Attanasio, M., Zhou, W., Chaki, M., Paruchuri, Y., Wise, E.L., Wolf, M.T., Utsch, B., Becker, C. *et al.* (2009) Hypomorphic mutations in meckelin (MKS3/TMEM67) cause nephronophthisis with liver fibrosis (NPHP11). *J. Med. Genet.*, **46**, 663–670.
30. Drummond, I.A. (2012) Cilia functions in development. *Curr. Opin. Cell Biol.*, **24**, 24–30.
31. Chih, B., Liu, P., Chinn, Y., Chalouni, C., Komuves, L.G., Hass, P.E., Sandoval, W. and Peterson, A.S. (2012) A ciliopathy complex at the transition zone protects the cilia as a privileged membrane domain. *Nat. Cell Biol.*, **14**, 61–72.
32. Shiba, D., Manning, D.K., Koga, H., Beier, D.R. and Yokoyama, T. (2010) Inv acts as a molecular anchor for Nphp3 and Nek8 in the proximal segment of primary cilia. *Cytoskeleton*, **67**, 112–119.
33. Tammachote, R., Hommerding, C.J., Sinders, R.M., Miller, C.A., Czarnecki, P.G., Leightner, A.C., Salisbury, J.L., Ward, C.J., Torres, V.E., Gattone, V.H. 2nd *et al.* (2009) Ciliary and centrosomal defects associated with mutation and depletion of the Meckel syndrome genes MKS1 and MKS3. *Hum. Mol. Genet.*, **18**, 3311–3323.
34. Dawe, H.R., Smith, U.M., Cullinane, A.R., Gerrelli, D., Cox, P., Badano, J.L., Blair-Reid, S., Sriram, N., Katsanis, N., Attie-Bitach, T. *et al.* (2007) The Meckel-Gruber Syndrome proteins MKS1 and meckelin interact and are required for primary cilium formation. *Hum. Mol. Genet.*, **16**, 173–186.
35. Wallingford, J.B. and Mitchell, B. (2011) Strange as it may seem: the many links between Wnt signaling, planar cell polarity, and cilia. *Genes Dev.*, **25**, 201–213.
36. Lancaster, M.A. and Gleeson, J.G. (2010) Cystic kidney disease: the role of Wnt signaling. *Trends Mol. Med.*, **16**, 349–360.
37. Kim, I., Ding, T., Fu, Y., Li, C., Cui, L., Li, A., Lian, P., Liang, D., Wang, D.W., Guo, C. *et al.* (2009) Conditional mutation of Pkd2 causes cystogenesis and upregulates beta-catenin. *J. Am. Soc. Nephrol.*, **20**, 2556–2569.
38. Corbit, K.C., Shyer, A.E., Dowdle, W.E., Gaulden, J., Singla, V., Chen, M.H., Chuang, P.T. and Reiter, J.F. (2008) Kif3a constrains beta-catenin-dependent Wnt signalling through dual ciliary and non-ciliary mechanisms. *Nat. Cell Biol.*, **10**, 70–76.
39. Lancaster, M.A., Schroth, J. and Gleeson, J.G. (2011) Subcellular spatial regulation of canonical Wnt signalling at the primary cilium. *Nat. Cell Biol.*, **13**, 700–707.
40. Saadi-Kheddouci, S., Berrebi, D., Romagnolo, B., Cluzeaud, F., Peuchmaur, M., Kahn, A., Vandewalle, A. and Perret, C. (2001) Early development of polycystic kidney disease in transgenic mice expressing an activated mutant of the beta-catenin gene. *Oncogene*, **20**, 5972–5981.
41. Goodrich, L.V. and Strutt, D. (2011) Principles of planar polarity in animal development. *Development*, **138**, 1877–1892.
42. McNeill, H. (2009) Planar cell polarity and the kidney. *J. Am. Soc. Nephrol.*, **20**, 2104–2111.
43. Jones, C., Roper, V.C., Foucher, I., Qian, D., Banizs, B., Petit, C., Yoder, B.K. and Chen, P. (2008) Ciliary proteins link basal body polarization to planar cell polarity regulation. *Nat. Genet.*, **40**, 69–77.
44. Simons, M. and Mlodzik, M. (2008) Planar cell polarity signaling: from fly development to human disease. *Annu. Rev. Genet.*, **42**, 517–540.
45. Karner, C., Wharton, K.A. Jr and Carroll, T.J. (2006) Planar cell polarity and vertebrate organogenesis. *Semin. Cell Dev. Biol.*, **17**, 194–203.
46. Jones, C. and Chen, P. (2007) Planar cell polarity signaling in vertebrates. *Bioessays*, **29**, 120–132.
47. Baena-Lopez, L.A., Baonza, A. and Garcia-Bellido, A. (2005) The orientation of cell divisions determines the shape of Drosophila organs. *Curr. Biol.*, **15**, 1640–1644.
48. Saburi, S., Hester, I., Fischer, E., Pontoglio, M., Eremina, V., Gessler, M., Quaggin, S.E., Harrison, R., Mount, R. and McNeill, H. (2008) Loss of Fat4 disrupts PCP signaling and oriented cell division and leads to cystic kidney disease. *Nat. Genet.*, **40**, 1010–1015.
49. Fischer, E., Legue, E., Doyen, A., Nato, F., Nicolas, J.F., Torres, V., Yaniv, M. and Pontoglio, M. (2006) Defective planar cell polarity in polycystic kidney disease. *Nat. Genet.*, **38**, 21–23.
50. Nishio, S., Tian, X., Gallagher, A.R., Yu, Z., Patel, V., Igarashi, P. and Somlo, S. (2010) Loss of oriented cell division does not initiate cyst formation. *J. Am. Soc. Nephrol.*, **21**, 295–302.
51. Cook, S.A., Collin, G.B., Bronson, R.T., Naggert, J.K., Liu, D.P., Akeson, E.C. and Davisson, M.T. (2009) A mouse model for Meckel syndrome type 3. *J. Am. Soc. Nephrol.*, **20**, 753–764.
52. Gattone, V.H. 2nd, Tourkow, B.A., Trambaugh, C.M., Yu, A.C., Whelan, S., Phillips, C.L., Harris, P.C. and Peterson, R.G. (2004) Development of multiorgan pathology in the wpk rat model of polycystic kidney disease. *Anat. Rec. A Discov. Mol. Cell Evol. Biol.*, **277**, 384–395.
53. Weatherbee, S.D., Niswander, L.A. and Anderson, K.V. (2009) A mouse model for Meckel syndrome reveals Mks1 is required for ciliogenesis and Hedgehog signaling. *Hum. Mol. Genet.*, **18**, 4565–4575.
54. Cui, C., Chatterjee, B., Francis, D., Yu, Q., SanAgustin, J.T., Francis, R., Tansey, T., Henry, C., Wang, B., Lemley, B. *et al.* (2011) Disruption of Mks1 localization to the mother centriole causes cilia defects and developmental malformations in Meckel-Gruber syndrome. *Dis. Model Mech.*, **4**, 43–56.
55. Adams, M., Simms, R.J., Abdelhamed, Z., Dawe, H.R., Szymanska, K., Logan, C.V., Wheway, G., Pitt, E., Gull, K., Knowles, M.A. *et al.* (2012) A meckelin-filamin A interaction mediates ciliogenesis. *Hum. Mol. Genet.*, **21**, 1272–1286.
56. Ross, A.J., May-Simera, H., Eichers, E.R., Kai, M., Hill, J., Jagger, D.J., Leitch, C.C., Chapple, J.P., Munro, P.M., Fisher, S. *et al.* (2005) Disruption of Bardet-Biedl syndrome ciliary proteins perturbs planar cell polarity in vertebrates. *Nat. Genet.*, **37**, 1135–1140.
57. Montcouquiol, M., Rachel, R.A., Lanford, P.J., Copeland, N.G., Jenkins, N.A. and Kelley, M.W. (2003) Identification of Vangl2 and Scrb1 as planar polarity genes in mammals. *Nature*, **423**, 173–177.
58. Wang, J., Mark, S., Zhang, X., Qian, D., Yoo, S.J., Radde-Gallwitz, K., Zhang, Y., Lin, X., Collazo, A., Wynshaw-Boris, A. *et al.* (2005)

Regulation of polarized extension and planar cell polarity in the cochlea by the vertebrate PCP pathway. *Nat. Genet.*, **37**, 980–985.
59. Sipe, C.W. and Lu, X. (2011) Kif3a regulates planar polarization of auditory hair cells through both ciliary and non-ciliary mechanisms. *Development*, **138**, 3441–3449.
60. Wang, Y., Guo, N. and Nathans, J. (2006) The role of Frizzled3 and Frizzled6 in neural tube closure and in the planar polarity of inner-ear sensory hair cells. *J. Neurosci.*, **26**, 2147–2156.
61. Reed, W., Avolio, J. and Satir, P. (1984) The cytoskeleton of the apical border of the lateral cells of freshwater mussel gill: structural integration of microtubule and actin filament-based organelles. *J. Cell Sci.*, **68**, 1–33.
62. Guirao, B., Meunier, A., Mortaud, S., Aguilar, A., Corsi, J.M., Strehl, L., Hirota, Y., Desoeuvre, A., Boutin, C., Han, Y.G. *et al.* (2010) Coupling between hydrodynamic forces and planar cell polarity orients mammalian motile cilia. *Nat. Cell Biol.*, **12**, 341–350.
63. Park, T.J., Mitchell, B.J., Abitua, P.B., Kintner, C. and Wallingford, J.B. (2008) Dishevelled controls apical docking and planar polarization of basal bodies in ciliated epithelial cells. *Nat. Genet.*, **40**, 871–879.
64. Wallingford, J.B. (2010) Planar cell polarity signaling, cilia and polarized ciliary beating. *Curr. Opin. Cell. Biol.*, **22**, 597–604.
65. Germino, G.G. (2005) Linking cilia to Wnts. *Nat. Genet.*, **37**, 455–457.
66. Simons, M. and Walz, G. (2006) Polycystic kidney disease: cell division without a c(l)ue? *Kidney Int.*, **70**, 854–864.
67. Gerdes, J.M., Liu, Y., Zaghloul, N.A., Leitch, C.C., Lawson, S.S., Kato, M., Beachy, P.A., Beales, P.L., DeMartino, G.N., Fisher, S. *et al.* (2007) Disruption of the basal body compromises proteasomal function and perturbs intracellular Wnt response. *Nat. Genet.*, **39**, 1350–1360.
68. Leitch, C.C., Zaghloul, N.A., Davis, E.E., Stoetzel, C., Diaz-Font, A., Rix, S., Alfadhel, M., Lewis, R.A., Eyaid, W., Banin, E. *et al.* (2008) Hypomorphic mutations in syndromic encephalocele genes are associated with Bardet-Biedl syndrome. *Nat. Genet.*, **40**, 443–448.
69. Burckle, C., Gaude, H.M., Vesque, C., Silbermann, F., Salomon, R., Jeanpierre, C., Antignac, C., Saunier, S. and Schneider-Maunoury, S. (2011) Control of the Wnt pathways by nephrocystin-4 is required for morphogenesis of the zebrafish pronephros. *Hum. Mol. Genet.*, **20**, 2611–2627.
70. Otto, E.A., Schermer, B., Obara, T., O'Toole, J.F., Hiller, K.S., Mueller, A.M., Ruf, R.G., Hoefele, J., Beekmann, F., Landau, D. *et al.* (2003) Mutations in INVS encoding inversin cause nephronophthisis type 2, linking renal cystic disease to the function of primary cilia and left-right axis determination. *Nat. Genet.*, **34**, 413–420.
71. Zhou, W., Dai, J., Attanasio, M. and Hildebrandt, F. (2010) Nephrocystin-3 is required for ciliary function in zebrafish embryos. *Am. J. Physiol. Renal. Physiol.*, **299**, 55–62.
72. Tetsu, O. and McCormick, F. (1999) Beta-catenin regulates expression of cyclin D1 in colon carcinoma cells. *Nature*, **398**, 422–426.
73. He, T.C., Chan, T.A., Vogelstein, B. and Kinzler, K.W. (1999) PPARdelta is an APC-regulated target of nonsteroidal anti-inflammatory drugs. *Cell*, **99**, 335–345.
74. ten Berge, D., Brugmann, S.A., Helms, J.A. and Nusse, R. (2008) Wnt and FGF signals interact to coordinate growth with cell fate specification during limb development. *Development*, **135**, 3247–3257.
75. He, T.C., Sparks, A.B., Rago, C., Hermeking, H., Zawel, L., da Costa, L.T., Morin, P.J., Vogelstein, B. and Kinzler, K.W. (1998) Identification of c-MYC as a target of the APC pathway. *Science*, **281**, 1509–1512.
76. DasGupta, R. and Fuchs, E. (1999) Multiple roles for activated LEF/TCF transcription complexes during hair follicle development and differentiation. *Development*, **126**, 4557–4568.
77. Ferrante, M.I., Romio, L., Castro, S., Collins, J.E., Goulding, D.A., Stemple, D.L., Woolf, A.S. and Wilson, S.W. (2009) Convergent extension movements and ciliary function are mediated by ofd1, a zebrafish orthologue of the human oral-facial-digital type 1 syndrome gene. *Hum. Mol. Genet.*, **18**, 289–303.
78. Simons, M., Gloy, J., Ganner, A., Bullerkotte, A., Bashkurov, M., Kronig, C., Schermer, B., Benzing, T., Cabello, O.A., Jenny, A. *et al.* (2005) Inversin, the gene product mutated in nephronophthisis type II, functions as a molecular switch between Wnt signaling pathways. *Nat. Genet.*, **37**, 537–543.
79. Kimmel, C.B., Ballard, W.W., Kimmel, S.R., Ullmann, B. and Schilling, T.F. (1995) Stages of embryonic development of the zebrafish. *Dev. Dyn.*, **203**, 253–310.
80. Angers, S., Thorpe, C.J., Biechele, T.L., Goldenberg, S.J., Zheng, N., MacCoss, M.J. and Moon, R.T. (2006) The KLHL12-Cullin-3 ubiquitin ligase negatively regulates the Wnt-beta-catenin pathway by targeting Dishevelled for degradation. *Nat. Cell Biol.*, **8**, 348–357.
81. Thorpe, C.J., Weidinger, G. and Moon, R.T. (2005) Wnt/beta-catenin regulation of the Sp1-related transcription factor sp5l promotes tail development in zebrafish. *Development*, **132**, 1763–1772.
82. Jessen, J.R., Topczewski, J., Bingham, S., Sepich, D.S., Marlow, F., Chandrasekhar, A. and Solnica-Krezel, L. (2002) Zebrafish trilobite identifies new roles for Strabismus in gastrulation and neuronal movements. *Nat. Cell Biol.*, **4**, 610–615.
83. Park, M. and Moon, R.T. (2002) The planar cell-polarity gene stbm regulates cell behaviour and cell fate in vertebrate embryos. *Nat. Cell Biol.*, **4**, 20–25.
84. Borovina, A., Superina, S., Voskas, D. and Ciruna, B. (2010) Vangl2 directs the posterior tilting and asymmetric localization of motile primary cilia. *Nat. Cell Biol.*, **12**, 407–412.
85. Collin, G.B., Won, J., Hicks, W.L., Cook, S.A., Nishina, P.M. and Naggert, J.K. (2012) Meckelin is necessary for photoreceptor intraciliary transport and outer segment morphogenesis. *Invest. Ophthalmol. Vis. Sci.*, **53**, 967–974.
86. Williams, C.L., Winkelbauer, M.E., Schafer, J.C., Michaud, E.J. and Yoder, B.K. (2008) Functional redundancy of the B9 proteins and nephrocystins in Caenorhabditis elegans ciliogenesis. *Mol. Biol. Cell*, **19**, 2154–2168.
87. Blitzer, A.L., Panagis, L., Gusella, G.L., Danias, J., Mlodzik, M. and Iomini, C. (2011) Primary cilia dynamics instruct tissue patterning and repair of corneal endothelium. *Proc. Natl Acad. Sci. USA*, **108**, 2819–2824.
88. Iglesias, D.M., Hueber, P.A., Chu, L., Campbell, R., Patenaude, A.M., Dziarmaga, A.J., Quinlan, J., Mohamed, O., Dufort, D. and Goodyer, P.R. (2007) Canonical WNT signaling during kidney development. *Am. J. Physiol. Renal. Physiol.*, **293**, 494–500.
89. Perantoni, A.O. (2003) Renal development: perspectives on a Wnt-dependent process. *Semin. Cell Dev. Biol.*, **14**, 201–208.
90. Calvet, J.P. (1994) Injury and development in polycystic kidney disease. *Curr. Opin. Nephrol. Hypertens.*, **3**, 340–348.
91. Lancaster, M.A., Louie, C.M., Silhavy, J.L., Sintasath, L., Decambre, M., Nigam, S.K., Willert, K. and Gleeson, J.G. (2009) Impaired Wnt-beta-catenin signaling disrupts adult renal homeostasis and leads to cystic kidney ciliopathy. *Nat. Med.*, **15**, 1046–1054.
92. Jonassen, J.A., SanAgustin, J., Baker, S.P. and Pazour, G.J. (2012) Disruption of IFT complex A causes cystic kidneys without mitotic spindle misorientation. *J. Am. Soc. Nephrol.*, **23**, 641–651.
93. Borgal, L., Habbig, S., Hatzold, J., Liebau, M.C., Dafinger, C., Sacarea, I., Hammerschmidt, M., Benzing, T. and Schermer, B. (2012) The ciliary protein nephrocystin-4 translocates the canonical Wnt regulator Jade-1 to the nucleus to negatively regulate beta-catenin signaling. *J. Biol. Chem.*, **287**, 25370–25380.
94. Wigley, W.C., Fabunmi, R.P., Lee, M.G., Marino, C.R., Muallem, S., DeMartino, G.N. and Thomas, P.J. (1999) Dynamic association of proteasomal machinery with the centrosome. *J. Cell Biol.*, **145**, 481–490.
95. Fischer, E. and Pontoglio, M. (2009) Planar cell polarity and cilia. *Semin. Cell Dev. Biol.*, **20**, 998–1005.
96. Phillips, C.L., Miller, K.J., Filson, A.J., Nurnberger, J., Clendenon, J.L., Cook, G.W., Dunn, K.W., Overbeek, P.A., Gattone, V.H. 2nd and Bacallao, R.L. (2004) Renal cysts of inv/inv mice resemble early infantile nephronophthisis. *J. Am. Soc. Nephrol.*, **15**, 1744–1755.
97. Rohde, L.A. and Heisenberg, C.P. (2007) Zebrafish gastrulation: cell movements, signals, and mechanisms. *Int. Rev. Cytol.*, **261**, 159–192.
98. Yin, C., Ciruna, B. and Solnica-Krezel, L. (2009) Convergence and extension movements during vertebrate gastrulation. *Curr. Top. Dev. Biol.*, **89**, 163–192.
99. Wang, Y. and Steinbeisser, H. (2009) Molecular basis of morphogenesis during vertebrate gastrulation. *Cell. Mol. Life Sci.*, **66**, 2263–2273.
100. Thisse, C. and Thisse, B. (2008) High-resolution in situ hybridization to whole-mount zebrafish embryos. *Nat. Protoc.*, **3**, 59–69.
101. Razidlo, D.F., Whitney, T.J., Casper, M.E., McGee-Lawrence, M.E., Stensgard, B.A., Li, X., Secreto, F.J., Knutson, S.K., Hiebert, S.W. and Westendorf, J.J. (2010) Histone deacetylase 3 depletion in osteo/chondroprogenitor cells decreases bone density and increases marrow fat. *PloS ONE*, **5**, e11492.